

Journal of Mechanics of Materials and Structures

**MULTI-REGION TREFFTZ COLLOCATION GRAINS (MTCGS)
FOR MODELING PIEZOELECTRIC COMPOSITE AND POROUS MATERIALS
IN DIRECT AND INVERSE PROBLEMS**

Peter L. Bishay, Abdullah Alotaibi and Satya N. Atluri

Volume 9, No. 3

May 2014



MULTI-REGION TREFFTZ COLLOCATION GRAINS (MTCGS) FOR MODELING PIEZOELECTRIC COMPOSITE AND POROUS MATERIALS IN DIRECT AND INVERSE PROBLEMS

PETER L. BISHAY, ABDULLAH ALOTAIBI AND SATYA N. ATLURI

A simple and efficient method for modeling piezoelectric composite and porous materials to solve direct and inverse 2D problems is presented in this paper. The method is based on discretizing the problem domain into arbitrary polygonal-shaped regions that resemble the physical shapes of grains in piezoelectric polycrystalline materials, and utilizing the Trefftz solution functions derived from the Lekhnitskii formulation for piezoelectric materials, or for elastic dielectric materials, to express the mechanical and electrical fields in the interior of each grain or region. A simple collocation method is used to enforce the continuity of the inter-region primary and secondary fields, as well as the essential and natural boundary conditions. Each region may contain a void, an elastic dielectric inclusion, or a piezoelectric inclusion. The void/inclusion interface conditions are enforced using the collocation method, or using the special solution set which is available only for the case of voids (traction-free, charge-free boundary conditions). The potential functions are written in terms of Laurent series which can describe interior or exterior domains, while the negative exponents are used only in the latter case. Because Lekhnitskii's solution for piezoelectric materials breaks down if there is no coupling between mechanical and electrical variables, the paper presents this solution in a general form that can be used for coupled (piezoelectric) as well as uncoupled (elastic dielectric) materials. Hence, the matrix or the inclusion can be piezoelectric or elastic dielectric to allow modeling of different types of piezoelectric composites. The present method can be used for determining the meso/macro physical properties of these materials as well as for studying the mechanics of damage initiation at the micro level in such materials. The inverse formulation can be used for determining the primary and secondary fields over some unreachable boundaries in piezoelectric composites and devices; this enables direct numerical simulation (DNS) and health monitoring of such composites and devices. Several examples are presented to show the efficiency of the method in modeling different piezoelectric composite and porous materials in different direct and inverse problems.

1. Introduction and literature review

Piezoelectric composites possess some enhanced properties over monolithic piezoelectric materials that enable them to be used in different industrial applications. Bigger range of coupled properties, better acoustic properties or figures of merit, and less brittleness are among these enhanced properties. Both “subtractive” and “additive” approaches were used to develop piezoelectric composites where, in the “subtractive” approach, controlled porosity is induced in piezoelectric materials to form porous piezoelectric materials with reduced density [Li et al. 2003]. These porous piezoelectric materials found

Bishay is the corresponding author.

Keywords: piezoelectric, composites, porous, Trefftz, Lekhnitskii, Voronoi cells, void, inclusion, collocation, inverse problems.

applications such as miniature accelerometers, vibration sensors, contact microphones and hydrophones. Porous piezoelectric materials have several advantages such as lack of possibility of destructive chemical reactions between the piezoelectric ceramic and the second phase (the air) during production, ability to control pore size, shape and distribution, light weight compared to monolithic piezoelectric materials and other piezoelectric composites, reduced price of production compared to other piezoelectric composites, and low acoustic impedances compared to dense ceramics, hence they could be used to improve the mismatch of acoustic impedances at the interfaces of medical ultrasonic imaging devices or underwater sonar detectors [Kumar et al. 2006]. Porous ceramics are classified by the International Union of Pure and Applied Chemistry (IUPAC) according to their pore size (or diameter d) as follows: macroporous ($d > 50$ nm), meso-porous (2 nm $< d < 50$ nm), and microporous ($d < 2$ nm). Also, they are classified according to the pore geometry [Araki and Halloran 2005] as: foam, interconnected, pore spaces between particles, plates and fibers, and large or small pore networks.

On the other hand, in the “additive” approach, the effective properties of the composite are optimized by combining two or more constituents. The second phase is used to modulate the overall properties of piezoelectric composites and could be dielectric ceramic [Jin et al. 2003], metal [Li et al. 2001], polymer [Klicker et al. 1981], or another piezoelectric material. Piezoelectric ceramics are also used in smart composite materials where piezoelectric rods (fibers) or particles are embedded in an elastic matrix.

Analytical models for porous piezoelectric materials are only available for simple geometries such as an infinite plate with circular or elliptical hole as presented in [Sosa 1991; Xu and Rajapakse 1999; Chung and Ting 1996; Lu and Williams 1998] using either the Lekhnitskii formalism [Lekhnitskii 1957] or the extended Stroh formalism [Stroh 1958]. However for more complicated geometries and practical problems, numerical methods such as finite elements, boundary elements, meshless or Trefftz methods should be used.

Modeling domains with defects (holes, inclusions or cracks) using the ordinary finite element method needs mesh refinement around defects in order to achieve acceptable results for the gradients of fields; hence it is very complex, time-consuming, and costly. Thus, special methods should be used to model defects. Special methods for direct numerical simulation (DNS) of micro/mesostructures were developed by Bishay and Atluri [2014] for porous piezoelectric materials; by Bishay et al. [2014] for piezoelectric composites; and by Dong and Atluri as 2D and 3D Trefftz cells [Dong and Atluri 2012b; 2012c; 2012d] and SGBEM cells [Dong and Atluri 2012e; 2013] for heterogeneous and functionally graded isotropic elastic materials, where each cell models an entire grain of the material, with elastic/rigid inclusions or voids, for direct numerical micromechanical analysis of composite and porous materials. Also 2D and 3D radial basis functions (RBF) grains were successfully used to model functionally graded materials (FGM) and the switching phenomena in ferroelectric materials by Bishay and Atluri [2012; 2013]. Finite elements with elliptical holes, inclusions or cracks in elastic materials were also developed by Zhang and Katsube [1995; 1997], Piltner [1985; 2008], and Wang and Qin [2012]. Hybrid-stress elements were developed by Ghosh and his coworkers (see [Moorthy and Ghosh 1996] for instance). Readers are referred to [Dong and Atluri 2012b] for a critical comparison between Ghosh’s hybrid-stress elements and the hybrid-displacement and Trefftz elements presented in the aforementioned papers. For piezoelectric materials, Wang et al. [2004] developed a hybrid finite element with a hole based on the Lekhnitskii formalism, while Cao et al. [2013] developed a hybrid finite element with defects based on the extended Stroh formalism. The boundary element method was also used by Xu and Rajapakse

[1998] to analyze piezoelectric materials with elliptical holes. In addition, Trefftz methods were used to model microstructures with defects, using multi-source-point Trefftz method in [Dong and Atluri 2012a] for plane elasticity, and Trefftz boundary collocation method for plane piezoelectricity macromechanics developed by Sheng et al. [2006] based on the Lekhnitskii formalism.

The basic idea of the various Trefftz methods is to use the so-called Trefftz functions which satisfy the homogenous governing equations of the relevant physical phenomenon as the trial and/or weight functions. A complete set of Trefftz functions that satisfy only the homogenous governing equations is termed as a *basic solution set*. A complete set of Trefftz functions that satisfy both the homogenous governing equations and the homogenous boundary conditions is termed as a *special solution set*. To formulate any Trefftz method, Trefftz functions must be available. For the case of impermeable voids, the *special solution set* that satisfies the traction-free, charge-free conditions can be used. Hence there is no need to enforce the void boundary conditions by collocation or any other method. Using the special solution set is more efficient. However, for the case of grains with pressurized voids or inclusions, the special solution set does not exist and collocation/least squares method should be used instead to enforce the void/inclusion boundary conditions.

In this paper, multi-region Trefftz collocation grains (MTCGs) are developed for modeling porous piezoelectric materials as well as piezoelectric composites where the materials of the matrix and the inclusion could be piezoelectric or elastic dielectric (anisotropic in general). The formulation is very simple and efficient since there are no simple polynomial-based elements in the finite element sense. Each grain has an arbitrarily polygonal shape to mimic the physical shape of grains in the microscale. Each grain may contain a circular or an arbitrarily oriented elliptical void or inclusion and has its own crystallographic orientation (poling direction). Each grain may be surrounded by an arbitrary number of neighboring grains; hence MTCGs are expected to show field distributions that cannot be obtained using regular triangular and four-sided polynomial-based finite elements. Dirichlet tessellation is used to construct the mesh or the geometric shapes of the grains. The formulation is also very effective in inverse problems where the boundary conditions over some portions of the problem boundary are completely unknown while on other portions extra conditions are known or measured. The Lekhnitskii formalism is employed here due to the relatively explicit nature of the derived Trefftz functions.

The paper is organized as follows: Section 2 introduces all governing equations and boundary conditions. Lekhnitskii's solution for coupled/uncoupled plane electroelastic problem is presented in Section 3 while the multi-region Trefftz collocation grains (MTCGs) formulation for piezoelectric composites with and without voids/inclusions is introduced in Section 4 for direct problems and in Section 5 for inverse problems. The advantage of using MTCGs to model representative volume element (RVE) for obtaining the overall material properties of piezoelectric composites is discussed in Section 6. Numerical examples are provided in Section 7 and conclusions are summarized in Section 8.

2. Governing equations and boundary conditions

Consider a domain Ω filled with a piezoelectric composite. On the boundary of the domain, denoted $\partial\Omega$, we can specify displacements on S_u or tractions on S_t (not both at any point, i.e., $S_u \cap S_t = \emptyset$). Similarly we can specify electric potential on S_φ or electric charge per unit area (electric displacement) on S_Q (where again $S_\varphi \cap S_Q = \emptyset$). So $\partial\Omega = S_u \cup S_t = S_\varphi \cup S_Q$. The whole domain Ω can be divided into N

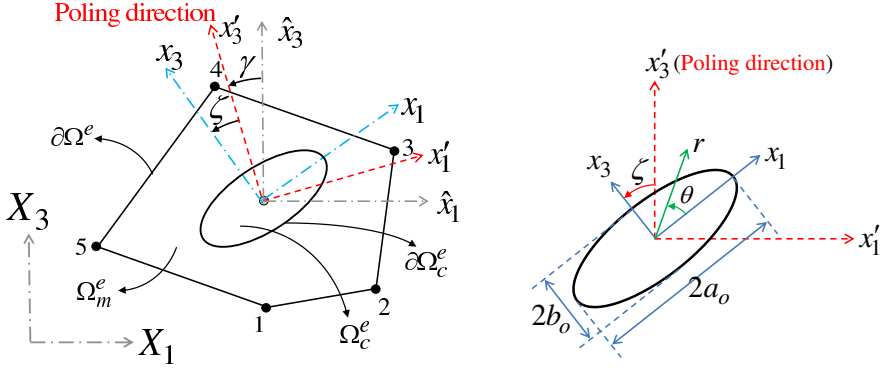


Figure 1. Left: 2D irregular polygon (grain) with an elliptical void/inclusion and its local coordinates (x_1-x_3) as well as the global (X_1-X_3) , grain local $(\hat{x}_1-\hat{x}_3)$ and crystallographic $(x'_1-x'_3)$ Cartesian coordinate systems. Right: elliptical void/inclusion with the local coordinate system as well as the poling direction of the piezoelectric material.

regions $\Omega = \sum_{e=1}^N \Omega^e$ (where each region may represent a grain in the material). The intersection of the boundary of region e , denoted $\partial\Omega^e$, with S_u, S_t, S_φ and S_Q is $S_u^e, S_t^e, S_\varphi^e$ and S_Q^e , while the intersection with the boundaries of the neighboring regions is denoted S_g^e . Hence $\partial\Omega^e = S_u^e \cup S_t^e \cup S_g^e = S_\varphi^e \cup S_Q^e \cup S_g^e$.

The domain of each region, Ω^e , may contain a void or an inclusion filling the domain Ω_c^e and has a boundary $\partial\Omega_c^e$ such that $\Omega_c^e \subset \Omega^e$ and $\partial\Omega_c^e \cap \partial\Omega^e = \emptyset$. In this case, the region outside the void/inclusion domain in region e is called the matrix domain $\Omega_m^e = \Omega^e - \Omega_c^e$. Figure 1 (left) shows one grain (irregular polygonal region for the 2D case) with an arbitrarily-oriented elliptical void/inclusion. The figure also shows the crystallographic coordinates and the poling direction.

Adopting matrix and vector notation and denoting \mathbf{u}^α (2 components), $\boldsymbol{\epsilon}^\alpha$ (3 components) and $\boldsymbol{\sigma}^\alpha$ (3 components) as the mechanical displacement vector, strain and stress tensors written in vector form respectively, and φ^α (scalar), \mathbf{E}^α (2 components) and \mathbf{D}^α (2 components) as the electric potential, electric field and electric displacement vectors respectively, where the superscript $\alpha = m$ or c (for matrix or inclusion), the following equations should be satisfied in the matrix and inclusion domains (Ω_m^e and Ω_c^e):

(1) Stress equilibrium and charge conservation (Gauss's) equations:

$$\partial_u^T \boldsymbol{\sigma}^\alpha + \bar{\mathbf{b}}^\alpha = \mathbf{0}; \quad \boldsymbol{\sigma}^\alpha = (\boldsymbol{\sigma}^\alpha)^T, \quad \partial_e^T \mathbf{D}^\alpha - \bar{\rho}_f^\alpha = 0, \tag{1}$$

where $\bar{\mathbf{b}}^\alpha$ is the body force vector, and $\bar{\rho}_f^\alpha$ is the electric free charge density (which is approximately zero for dielectric and piezoelectric materials).

(2) Strain-displacement (for infinitesimal deformations) and electric field-electric potential relations:

$$\boldsymbol{\epsilon}^\alpha = \partial_u \mathbf{u}^\alpha, \quad \mathbf{E}^\alpha = -\partial_e \varphi^\alpha, \tag{2}$$

where

$$\partial_u = \begin{bmatrix} \partial/\partial x_1 & 0 & \partial/\partial x_3 \\ 0 & \partial/\partial x_3 & \partial/\partial x_1 \end{bmatrix}^T, \quad \partial_e = [\partial/\partial x_1 \quad \partial/\partial x_3]^T.$$

The representation of the electric field in (2), as gradients of an electric potential, includes the assumption that Faraday's equation ($\nabla \times \mathbf{E}^\alpha = -\partial \mathbf{B}^\alpha / \partial t = \mathbf{0}$, where \mathbf{B} is the magnetic flux density) is satisfied

for electrostatics. Note that we consider only two equations (Gauss's and Faraday's equations) from the four Maxwell's equations. The remaining two equations (Gauss's law for magnetism and Ampere's law with Maxwell's correction) are not considered in the electrostatic analysis of piezoelectric materials.

(3) Piezoelectric material constitutive laws:

$$\begin{aligned} \boldsymbol{\sigma}^\alpha &= \mathbf{C}_E^\alpha \boldsymbol{\epsilon}^\alpha - \mathbf{e}^{\alpha T} \mathbf{E}^\alpha, & \boldsymbol{\epsilon}^\alpha &= \mathbf{S}_D^\alpha \boldsymbol{\sigma}^\alpha + \mathbf{g}^{\alpha T} \mathbf{D}^\alpha, \\ \mathbf{D}^\alpha &= \mathbf{e}^\alpha \boldsymbol{\epsilon}^\alpha + \mathbf{h}_\epsilon^\alpha \mathbf{E}^\alpha, & \text{or} & \quad \mathbf{E}^\alpha &= -\mathbf{g}^\alpha \boldsymbol{\sigma}^\alpha + \boldsymbol{\beta}_\sigma^\alpha \mathbf{D}^\alpha, \end{aligned} \quad (3)$$

where \mathbf{C}_E^α , $\mathbf{h}_\epsilon^\alpha$, \mathbf{S}_D^α , $\boldsymbol{\beta}_\sigma^\alpha$ are, respectively, the elastic stiffness tensor measured under constant electric field, dielectric permittivity tensor measured under constant strain, elastic compliance tensor measured under constant electric displacement, and inverse of the dielectric permittivity tensor measured under constant stress. \mathbf{e}^α and \mathbf{g}^α are piezoelectric tensors measured under constant strain and stress respectively.

The SI units of the mentioned fields are as follows: stress $\boldsymbol{\sigma}^\alpha$ (Pa or N/m²), strain $\boldsymbol{\epsilon}^\alpha$ (m/m), electric displacement \mathbf{D}^α (C/m²), electric field \mathbf{E}^α (V/m or N/C), and the SI units of the material matrices are: \mathbf{C}_E^α (Pa or N/m²), \mathbf{S}_D^α (m²/N), $\mathbf{h}_\epsilon^\alpha$ (C/Vm), $\boldsymbol{\beta}_\sigma^\alpha$ (Vm/C), \mathbf{e}^α (C/m²), and \mathbf{g}^α (m²/C). Note that $\mathbf{S}_D^\alpha \neq (\mathbf{C}_E^\alpha)^{-1}$ and $\boldsymbol{\beta}_\sigma^\alpha \neq (\mathbf{h}_\epsilon^\alpha)^{-1}$.

If the matrix or the inclusion material is elastic (not piezoelectric), then Equations (1) and (2) should be satisfied in the corresponding domains, and the coupling piezoelectric matrices $\mathbf{e}^\alpha = \mathbf{g}^\alpha = \mathbf{0}$ in (3).

2.1. Matrix boundary conditions.

(1) Mechanical natural (traction) and essential (displacement) boundary conditions:

$$\begin{aligned} \mathbf{n}_\sigma \boldsymbol{\sigma}^m &= \bar{\mathbf{t}} & \text{at } S_t \text{ or } S_t^e, \\ \mathbf{u}^m &= \bar{\mathbf{u}} & \text{at } S_u \text{ or } S_u^e, \end{aligned} \quad (4)$$

(2) Electric natural and essential boundary conditions:

$$\begin{aligned} \mathbf{n}_e \mathbf{D}^m &= \bar{Q} & \text{at } S_Q \text{ or } S_Q^e, \\ \varphi^m &= \bar{\varphi} & \text{at } S_\varphi \text{ or } S_\varphi^e. \end{aligned} \quad (5)$$

where

$$\mathbf{n}_\sigma = \begin{bmatrix} n_1 & 0 & n_3 \\ 0 & n_3 & n_1 \end{bmatrix}, \quad \mathbf{n}_e = [n_1 \quad n_3], \quad (6)$$

$\bar{\mathbf{t}}$ is the specified boundary traction vector, \bar{Q} is the specified surface density of free charge. n_1 and n_3 , the two components present in \mathbf{n}_σ and \mathbf{n}_e are the components of the unit outward normal to the grain boundary $\partial\Omega^e$. We designate $\bar{\mathbf{u}}$ as the specified mechanical displacement vector at the boundary S_u (or S_u^e), and $\bar{\varphi}$ as the specified electric potential at the boundary S_φ (or S_φ^e).

The following conditions should also be satisfied at each (inter-region) boundary S_g^e :

(1) Mechanical displacement and electric potential compatibility conditions:

$$\begin{aligned} \mathbf{u}^{m+} &= \mathbf{u}^{m-}, \\ \varphi^{m+} &= \varphi^{m-}. \end{aligned} \quad (7)$$

(2) Mechanical traction and electric charge reciprocity conditions:

$$\begin{aligned} (\mathbf{n}_\sigma \boldsymbol{\sigma}^m)^+ + (\mathbf{n}_\sigma \boldsymbol{\sigma}^m)^- &= 0, \\ (\mathbf{n}_e \mathbf{D}^m)^+ + (\mathbf{n}_e \mathbf{D}^m)^- &= 0. \end{aligned} \tag{8}$$

2.2. Impermeable void boundary conditions. The dielectric constants of piezoelectric materials are three orders of magnitude higher than that of air or vacuum inside the void. This means that charges do not accumulate on the void boundary and the impermeable assumption can be adopted. We then have *traction-free, charge-free* conditions along the void boundary $\partial\Omega_c^e$:

$$\begin{aligned} \mathbf{t}^m &= \mathbf{n}_\sigma \boldsymbol{\sigma}^m = \mathbf{0}, \\ Q^m &= \mathbf{n}_e \mathbf{D}^m = 0. \end{aligned} \tag{9}$$

2.3. Inclusion boundary conditions. If the matrix and inclusion materials are elastic and nonconducting (dielectric or piezoelectric), we have the following conditions along the inclusion boundary $\partial\Omega_c^e$:

(1) Mechanical displacement and electric potential continuity conditions:

$$\mathbf{u}^m = \mathbf{u}^c, \quad \varphi^m = \varphi^c. \tag{10}$$

(2) Traction reciprocity and charge continuity conditions:

$$-\mathbf{n}_\sigma \boldsymbol{\sigma}^m + \mathbf{n}_\sigma \boldsymbol{\sigma}^c = 0, \quad \mathbf{n}_e \mathbf{D}^m = \mathbf{n}_e \mathbf{D}^c, \tag{11}$$

where the normal unit vector whose components, n_1 and n_3 , appear in \mathbf{n}_e and \mathbf{n}_σ (see Equation (6)) along the inclusion boundary is directed away from the inclusion domain.

These inclusion boundary conditions can be used for the case of piezoelectric particles or fibers in a nonpiezoelectric matrix (polymer, say) or in a piezoelectric matrix made up of different material. They can also be used to model elastic particles or fibers in a piezoelectric matrix.

3. General solution of coupled/uncoupled plane electroelasticity using Lekhnitskii’s formulation

Let (x'_1, x'_3) be the principal material (crystallographic) coordinates, x'_3 be the poling direction (for piezoelectric materials) and (x_1, x_3) be the set of coordinates obtained by rotating (x'_1, x'_3) through an anti-clockwise rotation ζ (see Figure 1, right). Using the Lekhnitskii formalism [Lekhnitskii 1977], Xu and Rajapakse [1999] derived the general solution of plane piezoelectricity with respect to (x_1, x_3) coordinate system. This formulation is generalized here to be applicable to uncoupled electromechanical problems as for the case of isotropic or transversely-isotropic elastic dielectric materials (in the isotropic case, there is no unique crystallographic coordinate system; any coordinate system can be considered as such).

The constitutive equations with respect to the crystallographic axes $x'_1 - x'_3$ for plane stress and plane strain problems, with stress and electric displacement as objectives of the equations, can be written in compact form as:

$$\begin{Bmatrix} \boldsymbol{\epsilon}' \\ \mathbf{E}' \end{Bmatrix} = \begin{bmatrix} \mathbf{S}' & \mathbf{g}'^T \\ -\mathbf{g}' & \boldsymbol{\beta}' \end{bmatrix} \begin{Bmatrix} \boldsymbol{\sigma}' \\ \mathbf{D}' \end{Bmatrix}, \tag{12}$$

where superscripts, α , in (3) that indicate whether we are talking about the matrix or the inclusion, as well as the subscripts of \mathbf{S}' and $\boldsymbol{\beta}'$, are omitted for simplicity.

By invoking tensor transformation rule, the constitutive relations can be written with respect to (x_1, x_3) coordinate system as:

$$\begin{Bmatrix} \epsilon_1 \\ \epsilon_3 \\ \epsilon_5 \\ E_1 \\ E_3 \end{Bmatrix} = \begin{bmatrix} S_{11} & S_{13} & S_{15} & g_{11} & g_{31} \\ S_{13} & S_{33} & S_{35} & g_{13} & g_{33} \\ S_{15} & S_{35} & S_{55} & g_{15} & g_{35} \\ -g_{11} & -g_{13} & -g_{15} & \beta_{11} & \beta_{13} \\ -g_{31} & -g_{33} & -g_{35} & \beta_{13} & \beta_{33} \end{bmatrix} \begin{Bmatrix} \sigma_1 \\ \sigma_3 \\ \sigma_5 \\ D_1 \\ D_3 \end{Bmatrix} \quad \text{or} \quad \begin{Bmatrix} \boldsymbol{\epsilon} \\ \boldsymbol{E} \end{Bmatrix} = \begin{bmatrix} \boldsymbol{S} & \boldsymbol{g}^T \\ -\boldsymbol{g} & \boldsymbol{\beta} \end{bmatrix} \begin{Bmatrix} \boldsymbol{\sigma} \\ \boldsymbol{D} \end{Bmatrix}, \quad (13)$$

in which

$$\boldsymbol{S} = \boldsymbol{T}_2^T \boldsymbol{S}' \boldsymbol{T}_2, \quad \boldsymbol{g} = \boldsymbol{T}_1^T \boldsymbol{g}' \boldsymbol{T}_2, \quad \boldsymbol{\beta} = \boldsymbol{T}_1^T \boldsymbol{\beta}' \boldsymbol{T}_1, \quad (14)$$

and in the above equations,

$$\boldsymbol{T}_1 = \begin{bmatrix} \cos \zeta & -\sin \zeta \\ \sin \zeta & \cos \zeta \end{bmatrix} \quad \text{and} \quad \boldsymbol{T}_2 = \begin{bmatrix} \cos^2 \zeta & \sin^2 \zeta & -2 \sin \zeta \cos \zeta \\ \sin^2 \zeta & \cos^2 \zeta & 2 \sin \zeta \cos \zeta \\ \sin \zeta \cos \zeta & -\sin \zeta \cos \zeta & \cos^2 \zeta - \sin^2 \zeta \end{bmatrix}.$$

It can be seen that the coefficients \boldsymbol{S} , \boldsymbol{g} and $\boldsymbol{\beta}$ are functions of the angular rotation ζ . Again, for nonpiezoelectric materials, there is no coupling between the elastic and the electric fields, and $\boldsymbol{g}' = \boldsymbol{g} = \mathbf{0}$.

Here we summarize the expressions used to describe the primary and secondary fields in absence of body force and free-charge density ($\bar{\boldsymbol{b}} = \mathbf{0}$, $\bar{\rho}_f = 0$) using the Lekhnitskii formalism. For more details, the reader is referred to [Bishay and Atluri 2014; Sheng et al. 2006]. However, if the material is not piezoelectric and there is no coupling ($g_{ij} = 0$), the expressions presented in the aforementioned references break down. Hence, the following expressions are modified to account for both coupled and uncoupled materials:

$$\begin{Bmatrix} u_1 \\ u_3 \\ \varphi \end{Bmatrix} = 2 \operatorname{Re} \sum_{k=1}^3 \begin{Bmatrix} p_k \\ q_k / \mu_k \\ s_k \end{Bmatrix} \omega_k(z_k), \quad (15)$$

$$\begin{Bmatrix} \sigma_1 \\ \sigma_3 \\ \sigma_5 \end{Bmatrix} = 2 \operatorname{Re} \sum_{k=1}^3 \begin{Bmatrix} \gamma_k \mu_k^2 \\ \gamma_k \\ -\gamma_k \mu_k \end{Bmatrix} \omega'_k(z_k), \quad \begin{Bmatrix} D_1 \\ D_3 \end{Bmatrix} = 2 \operatorname{Re} \sum_{k=1}^3 \begin{Bmatrix} \lambda_k \mu_k \\ -\lambda_k \end{Bmatrix} \omega'_k(z_k),$$

$$\begin{Bmatrix} \epsilon_1 \\ \epsilon_3 \\ \epsilon_5 \end{Bmatrix} = 2 \operatorname{Re} \sum_{k=1}^3 \begin{Bmatrix} p_k \\ q_k \\ r_k \end{Bmatrix} \omega'_k(z_k), \quad \begin{Bmatrix} E_1 \\ E_3 \end{Bmatrix} = -2 \operatorname{Re} \sum_{k=1}^3 \begin{Bmatrix} s_k \\ t_k \end{Bmatrix} \omega'_k(z_k), \quad (16)$$

where $z_k = x_1 + \mu_k x_3$, $\omega_k(z_k)$ are three complex potential functions, the prime denotes differentiation with respect to z_k and

$$\begin{aligned} p_k &= \gamma_k (S_{11} \mu_k^2 + S_{13} - S_{15} \mu_k) + \lambda_k (g_{11} \mu_k - g_{31}), \\ q_k &= \gamma_k (S_{13} \mu_k^2 + S_{33} - S_{35} \mu_k) + \lambda_k (g_{13} \mu_k - g_{33}), \\ r_k &= \gamma_k (S_{15} \mu_k^2 + S_{15} - S_{55} \mu_k) + \lambda_k (g_{15} \mu_k - g_{35}), \\ s_k &= \gamma_k (g_{11} \mu_k^2 + g_{13} - g_{15} \mu_k) - \lambda_k (\beta_{11} \mu_k - \beta_{31}), \\ t_k &= \gamma_k (g_{31} \mu_k^2 + g_{33} - g_{35} \mu_k) - \lambda_k (\beta_{13} \mu_k - \beta_{33}), \end{aligned}$$

$$\lambda_k = \frac{g_{11}\mu_k^3 - (g_{15} + g_{31})\mu_k^2 + (g_{13} + g_{35})\mu_k - g_{33}}{\beta_{11}\mu_k^2 - 2\beta_{13}\mu_k + \beta_{33}}, \quad \gamma_k = 1 \quad \text{for piezoelectric material,}$$

$$\lambda_k = \delta_{k3}, \quad \gamma_k = \delta_{k1} + \delta_{k2} \quad \text{for nonpiezoelectric material,}$$

where δ_{ij} is the Kronecker delta. For piezoelectric materials, μ_k ($k = 1, \dots, 6$) are the roots of the characteristic equation

$$c_6\mu^6 + c_5\mu^5 + c_4\mu^4 + c_3\mu^3 + c_2\mu^2 + c_1\mu + c_0 = 0, \tag{17}$$

where

$$\begin{aligned} c_0 &= S_{33}\beta_{33} + g_{33}^2, \\ c_1 &= -2S_{35}\beta_{33} - 2S_{33}\beta_{13} - 2g_{33}(g_{13} + g_{35}), \\ c_2 &= S_{33}\beta_{11} + 4S_{35}\beta_{13} + \beta_{33}(2S_{13} + S_{55}) + 2g_{33}(g_{31} + g_{15}) + (g_{13} + g_{35})^2, \\ c_3 &= -2g_{11}g_{33} - 2S_{15}\beta_{33} - 2S_{35}\beta_{11} - 2\beta_{13}(2S_{13} + S_{55}) - 2(g_{31} + g_{15})(g_{13} + g_{35}), \\ c_4 &= S_{11}\beta_{33} + 4S_{15}\beta_{13} + \beta_{11}(2S_{13} + S_{55}) + 2g_{11}(g_{13} + g_{35}) + (g_{31} + g_{15})^2, \\ c_5 &= -2S_{11}\beta_{13} - 2S_{15}\beta_{11} - 2g_{11}(g_{31} + g_{15}), \\ c_6 &= S_{11}\beta_{11} + g_{11}^2, \end{aligned}$$

while for elastic dielectric materials, μ_1, μ_2, μ_4 and μ_5 are obtained from the elasticity equation (18), and μ_3 and μ_6 are obtained from the electrostatics equation (19):

$$S_{11}\mu^4 - 2S_{15}\mu^3 + (2S_{13} + S_{55})\mu^2 - 2S_{35}\mu^3 + S_{33} = 0, \tag{18}$$

$$\beta_{11}\mu^2 - 2\beta_{13}\mu + \beta_{33} = 0. \tag{19}$$

In general, the roots of (17) or those of (18) and (19) are complex with three conjugate pairs:

$$\mu_1 = A_{\mu 1} + iB_{\mu 1}, \quad \mu_2 = A_{\mu 2} + iB_{\mu 2}, \quad \mu_3 = A_{\mu 3} + iB_{\mu 3}, \quad \mu_4 = \bar{\mu}_1, \quad \mu_5 = \bar{\mu}_2, \quad \mu_6 = \bar{\mu}_3, \tag{20}$$

in which $i = \sqrt{-1}$, $A_{\mu k}$ and $B_{\mu k}$ ($k = 1, 2, 3$) are all distinct. Over-bar denotes complex conjugate.

3.1. Basic solution sets. For an elliptical void/inclusion as shown in Figure 1(right), the following conformal mapping can be used to transform an ellipse in z_k -plane into a unit circle in ξ_k -plane [Lekhnitskii 1977]:

$$\xi_k = \frac{z_k \pm \sqrt{z_k^2 - (a_o^2 + \mu_k^2 b_o^2)}}{a_o - i\mu_k b_o}, \quad k = 1, 2, 3, \tag{21}$$

where a_o and b_o are the half lengths of the void/inclusion axes as shown in Figure 1 (right) and the sign of the square root (\pm) is chosen in such a way that $|\xi_k| \geq 1$. The inverse mapping has the form

$$z_k = \frac{a_o - i\mu_k b_o}{2}\xi_k + \frac{a_o + i\mu_k b_o}{2}\xi_k^{-1}, \quad k = 1, 2, 3. \tag{22}$$

Along the void/inclusion boundary which is a unit circle in the ξ_k -plane, we have $|\xi_k| = 1$ or $\xi_1 = \xi_2 = \xi_3 = e^{i\Theta}$ where $\Theta \in [-\pi, \pi]$.

The *basic set* of Trefftz functions for electromechanical displacements $\underline{\mathbf{u}} = \{u_1, u_3, \varphi\}^T$, electromechanical stresses and strains $\underline{\boldsymbol{\sigma}} = \{\sigma_1 \ \sigma_3 \ \sigma_5 \ D_1 \ D_3\}^T$, $\underline{\boldsymbol{\epsilon}} = \{\epsilon_1 \ \epsilon_3 \ \epsilon_5 \ E_1 \ E_3\}^T$ for interior or exterior domains, respectively, can be obtained as

$$\underline{\mathbf{u}} = 2 \sum_{n=M_s}^M \sum_{k=1}^3 \left[(\operatorname{Re} \mathcal{D}_k \operatorname{Re} Z_k^n - \operatorname{Im} \mathcal{D}_k \operatorname{Im} Z_k^n) a_k^{(n)} - (\operatorname{Re} \mathcal{D}_k \operatorname{Im} Z_k^n + \operatorname{Im} \mathcal{D}_k \operatorname{Re} Z_k^n) b_k^{(n)} \right], \quad (23)$$

$$\underline{\boldsymbol{\sigma}} = 2 \sum_{n=M_s}^M \sum_{k=1}^3 \left[(\operatorname{Re} \mathcal{G}_k \operatorname{Re} n Y_k^{n-1} - \operatorname{Im} \mathcal{G}_k \operatorname{Im} n Y_k^{n-1}) a_k^{(n)} - (\operatorname{Re} \mathcal{G}_k \operatorname{Im} n Y_k^{n-1} + \operatorname{Im} \mathcal{G}_k \operatorname{Re} n Y_k^{n-1}) b_k^{(n)} \right], \quad (24)$$

$$\underline{\boldsymbol{\epsilon}} = 2 \sum_{n=M_s}^M \sum_{k=1}^3 \left[(\operatorname{Re} \mathcal{H}_k \operatorname{Re} n Y_k^{n-1} - \operatorname{Im} \mathcal{H}_k \operatorname{Im} n Y_k^{n-1}) a_k^{(n)} - (\operatorname{Re} \mathcal{H}_k \operatorname{Im} n Y_k^{n-1} + \operatorname{Im} \mathcal{H}_k \operatorname{Re} n Y_k^{n-1}) b_k^{(n)} \right]. \quad (25)$$

In the above,

$$\begin{aligned} \mathcal{D}_k &= \{p_k, q_k/\mu_k, s_k\}^T, & \mathcal{G}_k &= \{\gamma_k \mu_k^2, \gamma_k, -\gamma_k \mu_k, \lambda_k \mu_k, -\lambda_k\}^T, \\ \mathcal{H}_k &= \{p_k, q_k, r_k, -s_k, -t_k\}^T, \end{aligned}$$

and

$$\begin{aligned} M_s &= 0, & Z_k &= z_k, & Y_k^{n-1} &= z_k^{n-1} && \text{for simply connected domains,} \\ M_s &= 0, & Z_k &= \xi_k, & Y_k^{n-1} &= \xi_k^{n-1} && \text{for ellipse-interior domains,} \\ M_s &= -M, & Z_k &= \xi_k, & Y_k^{n-1} &= \frac{\xi_k^{n-1}}{A - B \xi_k^{-2}} && \text{for ellipse-exterior domains,} \end{aligned}$$

where $A = \frac{1}{2}(a_o - i \mu_k b_o)$, $B = \frac{1}{2}(a_o + i \mu_k b_o)$.

For interior/exterior solutions, when M is increased by one, six/twelve Trefftz functions with their corresponding undetermined real coefficients $\{a_1^{(\pm n)}, b_1^{(\pm n)}, a_2^{(\pm n)}, b_2^{(\pm n)}, a_3^{(\pm n)}, b_3^{(\pm n)}\}$ are added to the solution. So the number of Trefftz functions m_T (which is also equivalent to the number of undetermined real coefficients) is:

$$m_T = \begin{cases} 6(M+1) & \text{for interior domain solution,} \\ 6(2M+1) & \text{for exterior domain solution.} \end{cases} \quad (26)$$

Because of the exponential growth of the term Z_k^n as n is increased, we introduce a characteristic length to scale the Trefftz solution set in order to prevent the system of equations from being ill-conditioned. For an arbitrary polygonal grain as shown in [Figure 1](#) (left), where the coordinates of the nodes are (x_1^j, x_3^j) , $j = 1, 2, \dots, m$, the center point of the polygon has coordinates (x_1^c, x_3^c) . Relative to the local coordinates at the center point, we have $\hat{z}_k = \hat{x}_1 + \mu_k \hat{x}_3 = (x_1 - x_1^c) + \mu_k (x_3 - x_3^c)$, $k = 1, 2, 3$ and correspondingly,

$$\hat{\xi}_k = \frac{\hat{z}_k \pm \sqrt{\hat{z}_k^2 - (a_o^2 + \mu_k^2 b_o^2)}}{a_o - i \mu_k b_o}.$$

Now, Z_k (z_k for interior domains or ξ_k for exterior domains) will be replaced by \hat{Z}_k/R_c where

$$R_c = \max(R_{ck}), \quad R_{ck} = \max_j \sqrt{[\operatorname{Re} \hat{Z}_k^j]^2 + [\operatorname{Im} \hat{Z}_k^j]^2}, \quad j = 1, 2, \dots, m. \quad (27)$$

This is done only for terms with positive exponents. In this way, the exponential growth of Z_k^n is prevented as n is increased because $0 < |(\hat{Z}_k/R_c)^n| < 1$ for any point within the grain or along the grain boundaries.

3.2. Special solution set for impermeable elliptical voids. Trefftz special solution set accounts for the homogeneous boundary conditions of voids, cracks, etc. Wang et al. [2004] constructed a special solution set of Trefftz functions for elliptical voids with axes parallel/perpendicular to poling direction. Sheng et al. [2006] extended this to the case of arbitrarily oriented impermeable elliptical voids.

By enforcing traction-free, charge-free boundary conditions along the void surface, we can express $a_k^{(-n)}$ and $b_k^{(-n)}$ in terms of $a_k^{(n)}$ and $b_k^{(n)}$, as (see [Stroh 1958])

$$a_k^{(-n)} = \sum_{j=1}^3 (\text{Re}(E_{kj})a_j^{(n)} - \text{Im}(E_{kj})b_j^{(n)}), \quad b_k^{(-n)} = - \sum_{j=1}^3 (\text{Im}(E_{kj})a_j^{(n)} + \text{Re}(E_{kj})b_j^{(n)}), \quad (28)$$

where

$$\begin{bmatrix} E_{11} & E_{12} & E_{13} \\ E_{21} & E_{22} & E_{23} \\ E_{31} & E_{32} & E_{33} \end{bmatrix} = - \begin{bmatrix} \gamma_1 & \gamma_2 & \gamma_3 \\ \gamma_1\bar{\mu}_1 & \gamma_2\bar{\mu}_2 & \gamma_3\bar{\mu}_3 \\ \bar{\lambda}_1 & \bar{\lambda}_2 & \bar{\lambda}_3 \end{bmatrix}^{-1} \begin{bmatrix} \gamma_1 & \gamma_2 & \gamma_3 \\ \gamma_1\mu_1 & \gamma_2\mu_2 & \gamma_3\mu_3 \\ \lambda_1 & \lambda_2 & \lambda_3 \end{bmatrix}.$$

So the number of Trefftz functions m_T (which is also equivalent to the number of undetermined real coefficients) is reduced to $m_T = 6(M + 1)$.

Substituting (28) into (23)–(25) yields the following *special set* of Trefftz functions:

$$\begin{aligned} \underline{u}_{\text{void}} &= \sum_{n=0}^M \sum_{k=1}^3 (\Phi_{a_k}^{(n)} a_k^{(n)} + \Phi_{b_k}^{(n)} b_k^{(n)}), \\ \underline{\sigma}_{\text{void}} &= \sum_{n=0}^M \sum_{k=1}^3 (\Psi_{a_k}^{(n)} a_k^{(n)} + \Psi_{b_k}^{(n)} b_k^{(n)}), \\ \underline{\epsilon}_{\text{void}} &= \sum_{n=0}^M \sum_{k=1}^3 (\Gamma_{a_k}^{(n)} a_k^{(n)} + \Gamma_{b_k}^{(n)} b_k^{(n)}), \end{aligned} \quad (29)$$

where

$$\begin{aligned} \Phi_{a_k}^{(n)} &= \chi_{a_k}^{(n)} + \sum_{j=1}^3 (\text{Re}(E_{jk})\chi_{a_j}^{(-n)} - \text{Im}(E_{jk})\chi_{b_j}^{(-n)}), \quad \Phi_{b_k}^{(n)} = \chi_{b_k}^{(n)} - \sum_{j=1}^3 (\text{Im}(E_{jk})\chi_{a_j}^{(-n)} + \text{Re}(E_{jk})\chi_{b_j}^{(-n)}), \\ \Psi_{a_k}^{(n)} &= \Sigma_{a_k}^{(n)} + \sum_{j=1}^3 (\text{Re}(E_{jk})\Sigma_{a_j}^{(-n)} - \text{Im}(E_{jk})\Sigma_{b_j}^{(-n)}), \quad \Psi_{b_k}^{(n)} = \Sigma_{b_k}^{(n)} - \sum_{j=1}^3 (\text{Im}(E_{jk})\Sigma_{a_j}^{(-n)} + \text{Re}(E_{jk})\Sigma_{b_j}^{(-n)}), \\ \Gamma_{a_k}^{(n)} &= \Upsilon_{a_k}^{(n)} + \sum_{j=1}^3 (\text{Re}(E_{jk})\Upsilon_{a_j}^{(-n)} - \text{Im}(E_{jk})\Upsilon_{b_j}^{(-n)}), \quad \Gamma_{b_k}^{(n)} = \Upsilon_{b_k}^{(n)} - \sum_{j=1}^3 (\text{Im}(E_{jk})\Upsilon_{a_j}^{(-n)} + \text{Re}(E_{jk})\Upsilon_{b_j}^{(-n)}), \end{aligned} \quad (30)$$

and in (30):

$$\begin{aligned} \chi_{a_k}^{(\pm n)} &= 2 \text{Re } \mathcal{D}_k \text{ Re } \xi_k^{\pm n} - 2 \text{Im } \mathcal{D}_k \text{ Im } \xi_k^{\pm n}, \\ \chi_{b_k}^{(\pm n)} &= -2 \text{Re } \mathcal{D}_k \text{ Im } \xi_k^{\pm n} - 2 \text{Im } \mathcal{D}_k \text{ Re } \xi_k^{\pm n}, \end{aligned}$$

$$\begin{aligned}\Sigma_{a_k}^{(\pm n)} &= \pm 2n \left(\operatorname{Re} \mathcal{G}_k \operatorname{Re} \frac{\xi_k^{\pm n-1}}{z'_k} - \operatorname{Im} \mathcal{G}_k \operatorname{Im} \frac{\xi_k^{\pm n-1}}{z'_k} \right), \\ \Sigma_{b_k}^{(\pm n)} &= \mp 2n \left(\operatorname{Re} \mathcal{G}_k \operatorname{Im} \frac{\xi_k^{\pm n-1}}{z'_k} + \operatorname{Im} \mathcal{G}_k \operatorname{Re} \frac{\xi_k^{\pm n-1}}{z'_k} \right), \\ \Upsilon_{a_k}^{(\pm n)} &= \pm 2n \left(\operatorname{Re} \mathcal{H}_k \operatorname{Re} \frac{\xi_k^{\pm n-1}}{z'_k} - \operatorname{Im} \mathcal{H}_k \operatorname{Im} \frac{\xi_k^{\pm n-1}}{z'_k} \right), \\ \Upsilon_{b_k}^{(\pm n)} &= \mp 2n \left(\operatorname{Re} \mathcal{H}_k \operatorname{Im} \frac{\xi_k^{\pm n-1}}{z'_k} + \operatorname{Im} \mathcal{H}_k \operatorname{Re} \frac{\xi_k^{\pm n-1}}{z'_k} \right).\end{aligned}$$

4. Multi-region Trefftz collocation grain (MTCGs) formulation for direct problems

Consider a 2D irregular m -sided polygonal grain with/without void/inclusion as shown in [Figure 1](#) (left). The basic solution set in Equations (23)–(25) can be used as the interior/exterior fields, which satisfy the constitutive law, the strain-displacement relationship, the electric field-electric potential relationship and the equilibrium and Maxwell's equations. For the case of impermeable elliptical voids, the special solution set in Equations (29) which additionally satisfies the void stress-free charge-free boundary conditions can be used instead. In matrix and vector notation, these interior/exterior fields in Ω^e when $\alpha = m$, and in Ω_c^e when $\alpha = c$, can be written in the form

$$\begin{Bmatrix} \mathbf{u}^\alpha \\ \varphi^\alpha \end{Bmatrix} = \begin{Bmatrix} N_u^\alpha \\ N_\varphi^\alpha \end{Bmatrix} \mathbf{c}^\alpha, \quad \begin{Bmatrix} \boldsymbol{\sigma}^\alpha \\ D^\alpha \end{Bmatrix} = \begin{Bmatrix} M_\sigma^\alpha \\ M_D^\alpha \end{Bmatrix} \mathbf{c}^\alpha, \quad (31)$$

or

$$\underline{\mathbf{u}}^\alpha = N^\alpha \mathbf{c}^\alpha, \quad \underline{\boldsymbol{\sigma}}^\alpha = M^\alpha \mathbf{c}^\alpha,$$

where N^α are the Trefftz functions in the order of $M_s, \dots, 0, 1, \dots, M$ and \mathbf{c}^α denotes the unknown real coefficients ($a_k^{(\pm n)}, b_k^{(\pm n)}$, $k = 1, 2, 3$ and $n = M_s, \dots, M$) associated with Trefftz functions. If there is no void/inclusion, only the nonnegative exponents are used in the basic solution set.

The tractions and density of free charge on the boundaries $\partial\Omega^e$ when $\alpha = m$, and $\partial\Omega_c^e$ when $\alpha = c$, can be written as

$$\mathbf{t}^\alpha = n_\sigma \boldsymbol{\sigma}^\alpha = n_\sigma M_\sigma^\alpha \mathbf{c}^\alpha, \quad Q = n_e D^\alpha = n_e M_D^\alpha \mathbf{c}^\alpha,$$

or

$$\underline{\mathbf{t}}^\alpha = \begin{Bmatrix} \mathbf{t}^\alpha \\ Q^\alpha \end{Bmatrix} = \begin{bmatrix} n_\sigma & \mathbf{0} \\ \mathbf{0} & n_e \end{bmatrix} \begin{Bmatrix} \boldsymbol{\sigma}^\alpha \\ D^\alpha \end{Bmatrix} = \underline{n} \boldsymbol{\sigma}^\alpha = \underline{n} M^\alpha \mathbf{c}^\alpha. \quad (32)$$

Now the following conditions should be enforced:

- (1) Continuities of primal fields (electromechanical displacements), in (7), as well as reciprocity conditions, in (8), at all boundaries, S_g^e , between a grain and its neighboring grains, if any.
- (2) Essential boundary conditions (in (4) and (5)) if prescribed on boundaries S_u^e and S_φ^e ,
- (3) Natural boundary conditions ((4) and (5)) if prescribed on boundaries S_t^e and S_Q^e .
- (4) Void/inclusion interface conditions as mentioned in [Section 2](#) (when an inclusion is present in the grain or when a void is present in the grain and the basic solution set is to be used).

In this work, we use the simple collocation/least squares method to enforce all these conditions. Galerkin method can also be used and may yield a slightly better accuracy, but it is more susceptible to round-off errors [Sheng et al. 2006] as compared to the straightforward collocation method. When the void/inclusion boundary $\partial\Omega_c^e$ shrinks to zero, the grain is reduced to the case of a grain with no void/inclusion.

For the case of an impermeable void, using the special solution set, which already satisfies the void traction-free charge-free boundary conditions, is clearly more efficient than using the basic set because there is no need to enforce any conditions on the void boundary, however if the void is pressurized, filled with conducting fluid or replaced by any type of inclusions, the basic set should be used as mentioned earlier (there is no special solution set in this case).

The first three of the aforementioned conditions are enforced in a strong sense at several preselected collocation points along the grain boundary $\partial\Omega^e$. n_c points, $(\mathbf{x}^{(r)}, r = 1, 2, \dots, n_c)$, are selected along each side of the grain's outer boundary. Also when using the basic solution set, (Equations (23)–(25)), void/inclusion boundary conditions are enforced by dividing the void/inclusion periphery into a number of curved segments, n_s , along the void/inclusion boundary $\partial\Omega_c^e = \sum_{j=1}^{n_s} \partial\Omega_{c_j}^e$, and enforcing the boundary conditions on each segment, or on the center point of each segment. So,

- (1) Continuity of electromechanical displacements and reciprocity of electromechanical tractions along S_g^{ab} , the boundary side that separates any two neighboring grains a and b :

$$\begin{aligned} \underline{\mathbf{u}}^m(\Omega^a)(\mathbf{x}^{(r)}, \mathbf{c}_a^m) - \underline{\mathbf{u}}^m(\Omega^b)(\mathbf{x}^{(r)}, \mathbf{c}_b^m) &= \mathbf{0}, & \mathbf{x}^{(r)} \in S_g^{ab}, & r = 1, 2, \dots, n_c, \\ \underline{\mathbf{t}}^m(\Omega^a)(\mathbf{x}^{(r)}, \mathbf{c}_a^m) + \underline{\mathbf{t}}^m(\Omega^b)(\mathbf{x}^{(r)}, \mathbf{c}_b^m) &= \mathbf{0}, & \mathbf{x}^{(r)} \in S_g^{ab}, & r = 1, 2, \dots, n_c. \end{aligned} \quad (33)$$

- (2) Essential boundary conditions along the boundaries S_u^e and S_φ^e in grain e :

$$\begin{aligned} \underline{\mathbf{u}}^m(\mathbf{x}^{(r)}, \mathbf{c}_e^m) &= \bar{\mathbf{u}}, & \mathbf{x}^{(r)} \in S_u^e, & r = 1, 2, \dots, n_c, \\ \underline{\varphi}^m(\mathbf{x}^{(r)}, \mathbf{c}_e^m) &= \bar{\varphi}, & \mathbf{x}^{(r)} \in S_\varphi^e, & r = 1, 2, \dots, n_c. \end{aligned} \quad (34)$$

- (3) Natural boundary conditions along the boundaries S_t^e and S_Q^e in grain e :

$$\begin{aligned} \underline{\mathbf{t}}^m(\mathbf{x}^{(r)}, \mathbf{c}_e^m) &= \bar{\mathbf{t}}, & \mathbf{x}^{(r)} \in S_t^e, & r = 1, 2, \dots, n_c, \\ \underline{Q}^m(\mathbf{x}^{(r)}, \mathbf{c}_e^m) &= \bar{Q}, & \mathbf{x}^{(r)} \in S_Q^e, & r = 1, 2, \dots, n_c. \end{aligned} \quad (35)$$

- (4) Void/inclusion interface conditions along $\partial\Omega_c^e$ (when using the basic solution set):

- (a) Impermeable void: traction-free and charge-free conditions along $\partial\Omega_c^e$:

$$\int_{\partial\Omega_{c_j}^e} \underline{\mathbf{t}}^m(\mathbf{x}, \mathbf{c}_e^m) ds = 0, \quad j = 1, 2, \dots, n_s. \quad (36)$$

- (b) Inclusion: primal fields' continuity, traction reciprocity and charge-continuity conditions along $\partial\Omega_c^e$:

$$\begin{aligned} \underline{\mathbf{u}}^m(\mathbf{x}^{(j)}, \mathbf{c}_e^m) - \underline{\mathbf{u}}^c(\mathbf{x}^{(j)}, \mathbf{c}_c^c) &= \mathbf{0}, & j &= 1, 2, \dots, n_s, \\ \underline{\mathbf{t}}^m(\mathbf{x}^{(j)}, \mathbf{c}_e^m) + \underline{\mathbf{t}}^c(\mathbf{x}^{(j)}, \mathbf{c}_c^c) &= \mathbf{0}, & j &= 1, 2, \dots, n_s. \end{aligned} \quad (37)$$

Combining all these conditions for N grains in a matrix/vector form leads to

$$\mathbf{A}\mathbf{c} = \mathbf{b} \quad \text{or} \quad \mathbf{c} = \mathbf{A}^{-1}\mathbf{b}, \quad (38)$$

where \mathbf{c} is a column matrix containing the unknown coefficients of the matrix and inclusion of all grains. The length of the vector \mathbf{c} can be expressed as

$$N_T = \sum_{e=1}^N ((m_T)_e + (m_{Tc})_e), \quad (39)$$

where $(m_T)_e$ is the number of Trefftz functions in the matrix of grain e , and $(m_{Tc})_e$ is the number of Trefftz functions in the inclusion of grain e (if applicable). These numbers depend on M , the highest order of Z_k in (23)–(25) or (29), used in the matrix and inclusion of each grain. In this study, we use the following (according to (26)):

$M = 4$ (for matrix of a grain with void or inclusion):

$$(m_T)_e = 6(2M + 1) = 54 \text{ (basic solution set, ellipse-exterior domain)}$$

$M = 4$ (for inclusions):

$$(m_{Tc})_e = 6(M + 1) = 30 \text{ (basic solution set, ellipse-interior domain)}$$

$M = 2$ (for matrix of a grain with impermeable void):

$$(m_T)_e = 6(M + 1) = 18 \text{ (special solution set).}$$

Since we are collocating six variables at each collocation point on each of the inner boundaries (boundaries shared by any two neighboring grains), and three variables at each collocation point on each of the outer boundaries (grain boundaries on the outer frame of the domain), the number of collocation equations can be expressed as:

$$N_E = n_c(6N_i + 3N_o) + \sum_{e=1}^N p_e(n_s)_e, \quad (40)$$

where N_i is the number of inner grain boundaries (sides) in the whole domain, N_o is the number of outer grain boundaries (sides) in the whole domain, and $(n_s)_e$ is the number of segments used to divide the void periphery in grain e (only if the basic solution set is used) or the number of collocation points along the inclusion periphery in grain e , and $p_e = 0$ if we are using the special solution set, $p_e = 3$ if grain e contains a void and the basic solution set is used, while $p_e = 6$ if grain e contains an inclusion.

In order for the system of equations (38) to be solved, we need $N_T \leq N_E$. In the last three examples we present in Section 7, we use two uniformly distributed collocation points on each side of the outer boundary of each grain ($n_c = 2$) and 16 points or segments on the void/inclusion boundary in each grain ($(n_s)_e = 16$). This ensures that the number of equations is larger than the number of unknowns; hence the system is over-constrained and is solved using singular value decomposition (SVD). The SVD method can solve even the singular system of equations and produces the least squares solutions to the over-constrained systems. The distribution of collocation points along each side of a grain's outer boundary could be selected as the Gaussian points [Bishay and Atluri 2012]. However this makes no significant difference in the solution.

5. Multi-region Trefftz collocation grain (MTCG) formulation for inverse problems with regularization

If both electromechanical displacements and tractions are specified or known only on a part of the problem boundary, the inverse problem is to determine the electromechanical displacements and tractions in the domain as well as the other part of the boundary where everything is unknown. The same can be said if “tractions” is replaced by “strains” in the previous sentence. One example is in health monitoring of piezoelectric composites and devices when data are known or measured on the outer boundaries, but not available at the inaccessible cavities in the domain.

Now let S_c^e be a part of the boundary of grain e (outer boundaries for a grain containing an inclusion, and both inner and outer boundaries for a grain with a void) where electromechanical displacements and tractions (or strains) are known. We use the available data and select enough collocation points ($\mathbf{x}^{(p)} \in S_c^e$, $p = 1, 2, \dots, P$) along S_c^e to get

$$\mathbf{u}^m(\mathbf{x}^{(p)}, \mathbf{c}_e^m) = \bar{\mathbf{u}}, \quad \varphi^m(\mathbf{x}^{(p)}, \mathbf{c}_e^m) = \bar{\varphi}, \quad p = 1, 2, \dots, P, \quad (41)$$

and

$$\mathbf{t}^m(\mathbf{x}^{(p)}, \mathbf{c}_e^m) = \bar{\mathbf{t}}, \quad Q^m(\mathbf{x}^{(p)}, \mathbf{c}_e^m) = \bar{Q}, \quad p = 1, 2, \dots, P, \quad (42)$$

or

$$\boldsymbol{\epsilon}^m(\mathbf{x}^{(p)}, \mathbf{c}_e^m) = \bar{\boldsymbol{\epsilon}}, \quad \mathbf{E}^m(\mathbf{x}^{(p)}, \mathbf{c}_e^m) = \bar{\mathbf{E}}, \quad p = 1, 2, \dots, P. \quad (43)$$

Combining (41) and (42) or (43) in addition to the continuity of electromechanical displacements and reciprocity of electromechanical tractions along S_g^{ab} in (33), and the inclusion boundary conditions in (37) for grains with inclusions, represent the measured or known data in all grains. This can be written in matrix form as

$$\mathbf{A}_I \mathbf{c}_I = \mathbf{b}_I. \quad (44)$$

This equation cannot be solved directly using the least squares method because the system of equations in inverse problems is known to be ill-posed and generally very-sensitive to perturbation in the measurement data on the boundary S_c^e . Hence, regularization techniques should be used to mitigate this ill-posedness. There are several regularization methods that were used in the literature, among which are the truncated singular value decomposition (TSVD), selective singular value decomposition (SSVD), and the Tikhonov regularization [Hansen 1994; Tikhonov and Arsenin 1974]. In this work, TSVD method was used and the regularization parameter is obtained using the generalized cross-validation (GCV) method. For details about the aforementioned methods, the reader is referred to [Hansen 1994].

This formulation is generally suitable for any selection of S_c^e . For a plate with a hole modeled with only one region ($N = e = 1$), for instance, S_c could be all or part of the outer boundary where all measurements can be taken.

6. On using representative volume element (RVE) to predict the effective material properties of piezoelectric composites

In order to determine the overall properties of piezoelectric composites from known properties of their constituents (matrix and particles or fibers), two approaches were used in the literature: macromechanical

and micromechanical. In the macromechanical approach, the heterogeneous structure of the composite is replaced by a homogeneous medium with anisotropic properties, while in the micromechanical approach, a periodic RVE or a unit cell model is used to obtain the global properties of the composite [Berger et al. 2006]. A unit cell is the smallest part that contains sufficient information on the geometrical and material parameters at the microscopic level to allow for prediction of the effective properties of the composite. The numerical methods, such as the finite elements, are well-suited to model the RVE and to describe the behavior of these composite materials because there are no restrictions on the geometry, the material properties, the number of phases, and the size of the composite constituents. When employing unit cell models, the local fields in the constituent phases can be accurately determined by the numerical method, and various mechanisms such as damage initiation and propagation can be studied through the analysis. Numerical homogenization method is based on finding a globally homogeneous medium equivalent to the original composite, where the strain energy stored in both systems is approximately the same. In order to do so, first, a representative volume element which captures the overall behavior of a composite structure is created. Then the effective material properties are calculated by applying periodic boundary conditions and appropriate load cases, which are connected to specific deformation patterns, to the unit cell [Kari et al. 2008].

It is known that the advantages of the analytical approaches over the FE analyses are their ability to model statistical distributions of fibers/particles in the composite, and their low computational time, while the FE analysis, in contrast, is appropriate for estimating the effective properties of composites with a given periodic fiber/particle distribution and more complicated geometries (different shapes of fibers' cross-section, more than two phases, etc.), and at the same time, the local fields can be obtained accurately. Berger et al. [2006] found that in order to get sufficiently accurate results from the FE model, the mesh density should be chosen in such a way that the average element width is at least 5% of the unit cell width. This means that at least 400 two-dimensional regular elements are required to accurately model a two-dimensional unit cell that includes only one fiber or particle. Finite element results are sensitive to mesh density; hence it could be a difficult task to find appropriate meshes for the RVE [Berger et al. 2005]. The disadvantages of the numerical models can be avoided if we resort to the newly developed techniques such as those presented in this article and in [Bishay and Atluri 2014; Bishay et al. 2014; Dong and Atluri 2012a; 2012b; 2012c; 2012d] because these advanced methods can model a grain with its inclusion using only one element or region whose geometric shape is arbitrary, hence any statistical random distribution of fibers or particles can be accounted for with relatively very small computational cost and with high resolution in local fields' calculation.

In Section 7.4, we show the ability of MTCGs method to predict the effective material properties of a piezoelectric composite using only one region, while in Section 7.5, we show the ability of the proposed method to model random distributions of the second phase, and to obtain high resolution of local fields that enables studying damage initiation mechanisms in the microlevel.

7. Numerical examples

The formulation described above is programmed using Matlab in a 64-bit Windows operating system, and executed on a PC computer equipped with Intel Q8300 2.5 GHz CPU, and 8 GB RAM. The material properties of the materials used in the examples in this section are listed in Table 1.

Property	C_{11}	C_{12}	C_{13}	C_{22}	C_{23}	C_{33}	C_{44}	C_{55}
PZT-4	139	77.8	74.3	139	74.3	113	25.3	25.3
PZT-7A	148	76.2	74.2	148	74.2	131	25.4	25.4
LaRC-SI	8.1	5.4	5.4	8.1	5.4	8.1	1.4	1.4
Property	C_{66}	e_{31}	e_{32}	e_{33}	e_{15}	h_{11}	h_{22}	h_{33}
PZT-4	30.6	-6.98	-6.98	13.84	13.44	6	6	5.47
PZT-7A	35.9	460	460	235	9.2	-2.1	-2.1	9.5
LaRC-SI	1.4	0	0	0	0	2.8	2.8	2.8

Table 1. Material properties used in the numerical examples: C_{ij} in GPa, e_{ij} in C/m², h_{ii} in pC/(Vm).

Simple problems that use grains with no voids or inclusions, such as patch test and bending of a piezoelectric panel, can be easily and accurately modeled using any number of grains (with no voids or inclusions) to mesh the problem domain, and the error in the whole structure is less than 1%. Patch test with any number of grains containing inclusions having the same material properties as that of the matrix can also be passed with error less than 1%.

In the following, we show some numerical examples using the proposed MTCGs. In the first example we present inverse problem where the electromechanical displacements and tractions are all measured with white noise on the outer boundary of a piezoelectric domain with an impermeable elliptical void under mechanical loading, and the variables on the unreachable void surface are predicted. Then we study the convergence of this inverse problem as the accessible part on the outer boundary of the domain shrinks. The problem of a piezoelectric inclusion in an infinite piezoelectric matrix is then studied. This is followed by evaluation of material properties of a piezoelectric particulate composite material as functions of particle volume fraction. Finally we present contour plots that detect damage-prone sites in porous piezoelectric material samples with arbitrary elliptical voids. Comparisons with other analytical and computational results are presented whenever possible.

7.1. Piezoelectric panel with impermeable void: inverse problem. Consider a piezoelectric panel with an arbitrarily oriented elliptical void whose semi-axes are a and b and the inclination angle between the elliptical void minor axis and the poling direction is ζ as shown in Figure 2 (left). The local coordinate system of the ellipse is denoted x_1 - x_3 , while the global coordinate system is denoted X_1 - X_3 . The poling direction is aligned with the global vertical X_3 axis (shown in blue in the figure). The material is PZT-4 whose properties are presented in Table 1 (taken from [Xu and Rajapakse 1999]) and plane strain assumption is used in this problem. Now consider that the electromechanical displacements and tractions are all measured at the outer boundary and that there is some white noise in the measurements. The inverse problem is to use these available measurements to predict the electromechanical tractions and displacements at the inner cavity. In this example, we use the analytical solution presented in [Xu and Rajapakse 1999] for an elliptical void in an infinite piezoelectric panel as the prescribed (or measured) data on the outer boundary after adding certain level of white noise. Mechanical load $\sigma_o = 1$ Pa is applied on the panel's upper and lower edges. In this example we take $L = W = 6a$, $b/a = 0.6$, $\zeta = 0$, $M = 4$

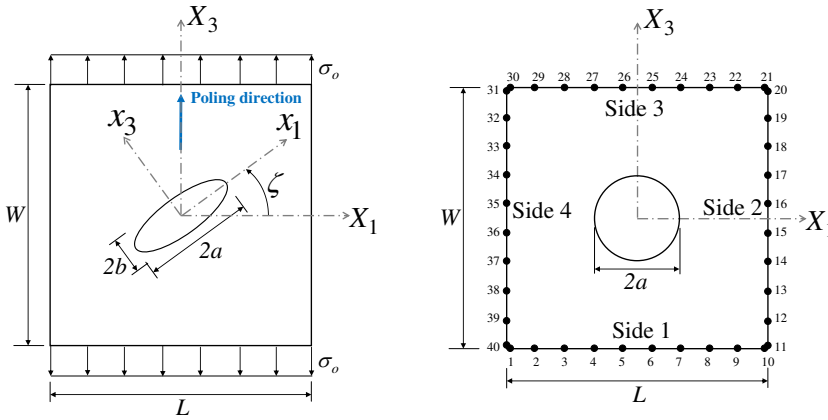


Figure 2. Left: a finite rectangular domain with arbitrarily oriented elliptical void. Right: collocation points considered in Section 7.2.

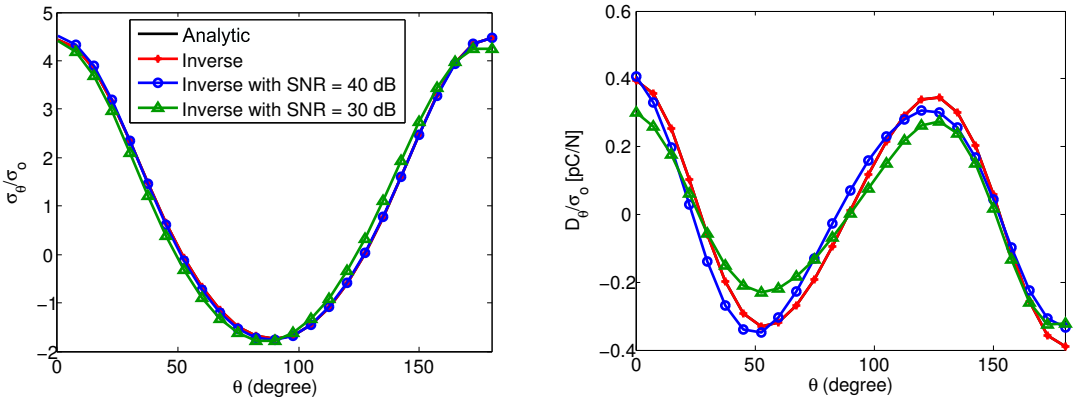


Figure 3. Variations of σ_θ/σ_o (left), D_θ/σ_o (right) along the periphery of an elliptical void.

(equivalent to 54 unknown coefficients) and we use 3 collocation points per side (giving 72 collocation equations). Hence, in this case S_c , mentioned in Section 5, is all the outer boundary of the plate where all data are measured.

Figure 3 and Figure 4 show the computed circumferential distributions of σ_θ , D_θ , E_θ and E_r divided by σ_o obtained from the solution of the inverse problem with different levels of white noise added to the measured electromechanical displacements and tractions. The figures show that when there is no noise present, this approach can always exactly reproduce the electromechanical tractions in the domain. When white noise of 40 dB and 30 dB signal-to-noise ratio (SNR), which is equivalent to 1% and 3.3% amplitude of noise in the measurements, is added, only limited error is obtained in the predicted stress, electric displacement and electric field on the void periphery.

The effects of varying ζ , a/b and W/a ratios on the stress, electric displacement and electric field are presented in [Xu and Rajapakse 1998].

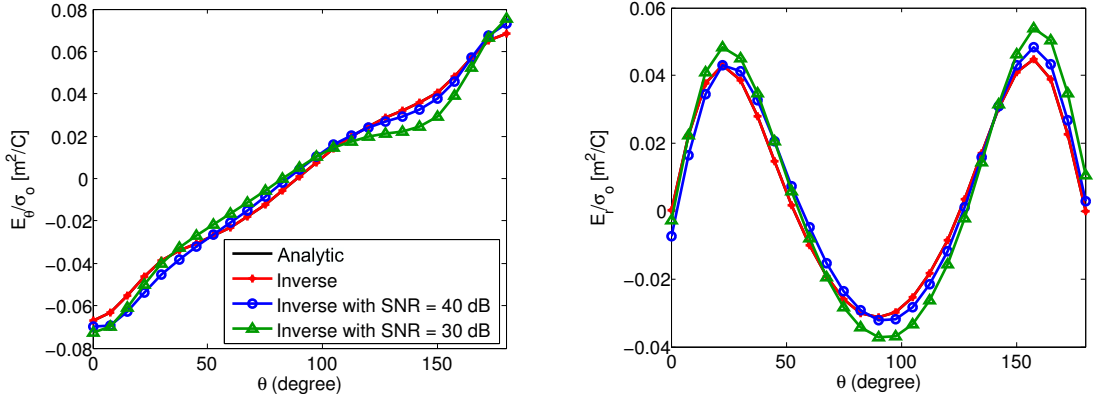


Figure 4. Variations of E_θ/σ_o (left), E_r/σ_o (right) along the periphery of an elliptical void.

7.2. Convergence study for the inverse problem. In this study, the same problem presented in Section 7.1 is considered again when the outer boundary is not fully accessible. Hence we rely on measurements taken from only a limited part of the outer boundary. Ten collocation points are used along each side of the outer boundary as shown in Figure 2 (right) and we keep removing collocation equations corresponding to these points from side 2 first (starting from point 11 in the figure) followed by side 3, then side 4. Every time we remove two points, we solve the problem and calculate the discrete extreme mechanical and electrical errors, expressed as

$$E_{\text{mech}} = \max_{\mathbf{x}_r \in \partial\Omega_c} \left(\frac{|\sigma_\theta(\mathbf{x}_r) - \tilde{\sigma}_\theta(\mathbf{x}_r)|}{\tilde{\sigma}_{\text{max}}} \right), \quad E_{\text{elect}} = \max_{\mathbf{x}_r \in \partial\Omega_c} \left(\frac{|D_\theta(\mathbf{x}_r) - \tilde{D}_\theta(\mathbf{x}_r)|}{\tilde{D}_{\text{max}}} \right), \quad (45)$$

where $\tilde{\sigma}_\theta(\mathbf{x}_r)$ and $\tilde{D}_\theta(\mathbf{x}_r)$ are the exact solutions at boundary points \mathbf{x}_r along the periphery of the void; $\tilde{\sigma}_{\text{max}}$ and \tilde{D}_{max} are respectively the maximum magnitudes of $\tilde{\sigma}_\theta(\mathbf{x}_r)$ and $\tilde{D}_\theta(\mathbf{x}_r)$.

It was found that when there is no noise in the prescribed (measured) data, only nine points (equivalent to 54 collocation equations, which is equal to the number of unknown coefficients when $M = 4$ is used) are required to get accurate results with E_{mech} and E_{elect} less than 0.001. These nine points could be prescribed on only a small part (quarter) of side 1 only, side 3 only, or on both sides 2 and 4 such that at least one point is on one of these two sides and the remaining points are on the other side. However when there is a white noise in the prescribed (measured) data, errors increase as we remove more points (or take our measurements from only a limited part of the outer boundary). The mechanical and electrical discrete extreme errors are presented in Table 2, when white noise of 40 dB signal-to-noise ratio (SNR) is added to the prescribed data, as more points are removed from the collocation points in Figure 2. It is clear from the table that the errors increase as more collocation points are removed from the outer boundary. When all collocation points on side 2 are not used, we get $E_{\text{mech}} \approx 3\%$, and $E_{\text{elect}} \approx 12\%$. When all collocation points on both side 2 and side 3 are not used, we get $E_{\text{mech}} \approx 17.5\%$, and $E_{\text{elect}} \approx 51\%$. Removing additional points from side 4, results in highly increasing E_{elect} .

It should be noted that the numbers in Table 2 change slightly every time we change the added random white noise. In addition, errors increase as the noise level increases.

Points removed	None	11–12	11–14	11–16	11–18	11–20	11–22
E_{mech}	0.0045	0.0106	0.0177	0.0225	0.0260	0.0297	0.0392
E_{elect}	0.0117	0.0525	0.0642	0.1030	0.1133	0.1207	0.1570
Points removed	11–24	11–26	11–28	11–30	11–32	11–34	11–36
E_{mech}	0.0423	0.0875	0.1004	0.1753	0.2807	0.4458	1.9738
E_{elect}	0.2393	0.2825	0.3373	0.5123	2.1058	5.4703	8.0255

Table 2. Discrete extreme mechanical and electrical errors as more collocation points are removed from the outer boundary (white noise of 40 dB SNR is added to the prescribed data on the outer boundary).

7.3. Infinite piezoelectric domain with elliptical inclusion. Consider an infinite piezoelectric plane with an elliptical inclusion subjected to vertical mechanical loading in the far field. For numerical implementations, the infinite domain is truncated into a rectangle with length L and width W , as shown in [Figure 2](#) (left) with $\zeta = 0$, $L = W = 6a$, and $\sigma_o = 1$ Pa. The matrix material is PZT-4 whose properties are presented in [Table 1](#) and plane strain assumption is used. The properties of the inclusion are given as:

$$\begin{bmatrix} \mathbf{C}_E^c & -\mathbf{e}^{cT} \\ \mathbf{e}^c & \mathbf{h}_\epsilon^c \end{bmatrix} = \Gamma \begin{bmatrix} \mathbf{C}_E^m & -\mathbf{e}^{mT} \\ \mathbf{e}^m & \mathbf{h}_\epsilon^m \end{bmatrix}, \quad (46)$$

where Γ is a factor that can be varied. $\Gamma > 1$ is equivalent to an inclusion material with stronger properties than those of the matrix material (larger stiffness, dielectric and piezoelectric material constants), while $\Gamma < 1$ is equivalent to an inclusion with weaker properties.

[Figure 5](#) shows the effect of b/a on σ_θ/σ_o , D_θ/σ_o , E_θ/σ_o and E_r/σ_o along the inclusion periphery with $\Gamma = 0.5$.

It can be seen from the figure that controlling the shape of the inclusions can result in varying the distribution and the maximum absolute values of the circumferential stress and electric displacement, as well as the circumferential and radial electric field, along the inclusion periphery. The effect of varying Γ on the aforementioned variables along the inclusion periphery is presented in [\[Bishay et al. 2014\]](#).

7.4. Evaluation of material properties of piezoelectric composites. Our 2D models can be used to estimate all effective material properties of composites with particles or voids, while for composites with fibers, only effective properties in the plane perpendicular to the fiber axis can be obtained. In this example, we determine the material properties of PZT-7A/LaRC-SI piezoelectric composite (PZT-7A piezoelectric particles embedded in LaRC-SI polyimide matrix) as functions of particle volume fraction. PZT-7A is a ceramic that exhibits the piezoelectric effect with electric fields applied along all three principle axes. LaRC-SI is a thermoplastic polyimide that was developed for aerospace applications. The material properties of all constituents are listed in [Table 1](#) (taken from [\[Odegard 2004\]](#)).

In order to calculate the effective material properties, computational models that ensure the presence of ϵ_{11} , ϵ_{33} , E_1 or E_3 alone in each model should be used. This is done by prescribing constant mechanical displacement or electric potential on the right or upper sides of the sample while enforcing zero electromechanical displacements on the other three sides. For more details about these computational models and how to calculate the effective material properties, the readers are referred to [\[Bishay and](#)

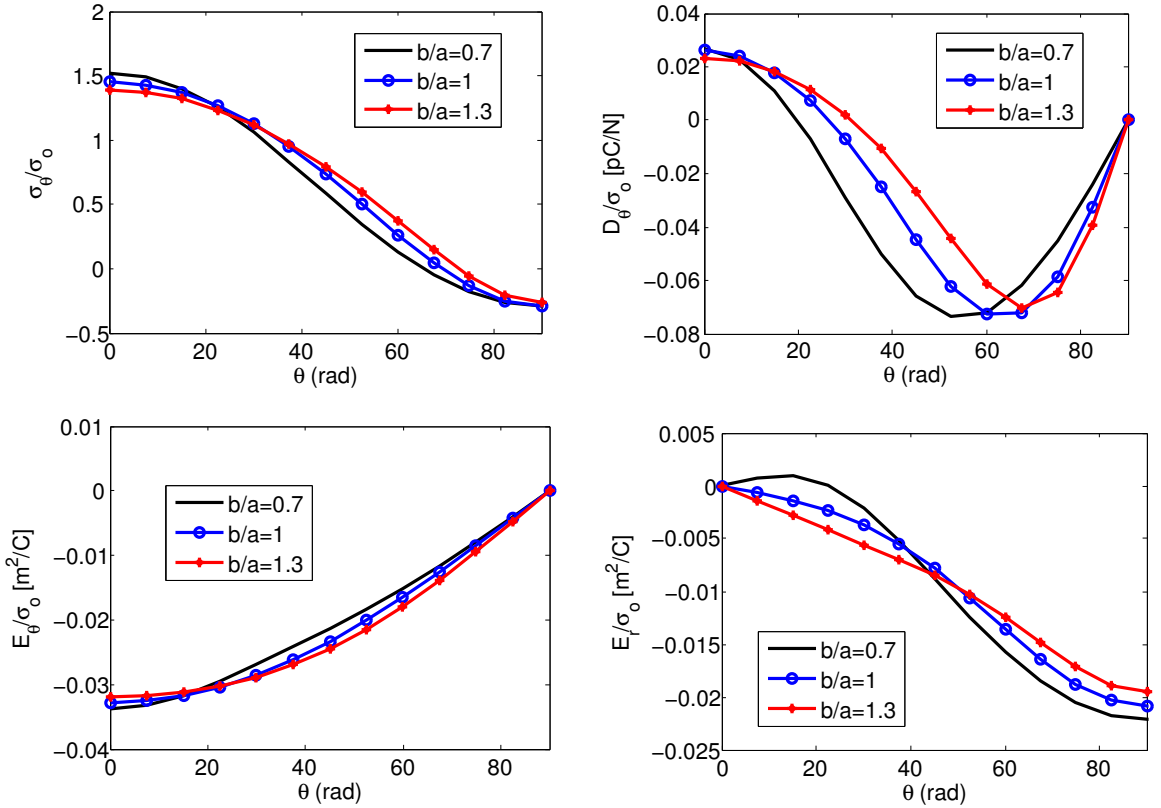


Figure 5. Effect of b/a on σ_θ/σ_o (top left), D_θ/σ_o (top right), E_θ/σ_o (bottom left) and E_r/σ_o (bottom right) along the inclusion periphery.

Atluri 2014]. Here we just present the results. The three Young's moduli Y_1 , Y_2 and Y_3 can be obtained from the stiffness matrix constants C_{ij} .

The RVE used is composed of just one region (grain) that includes an inclusion. Plane strain assumption is used in this study and the direction of polarization is vertically upward.

Figure 6 shows the predictions of the different effective material constants as functions of particle volume fraction and compared with Mori–Tanaka (MT), self-consistent (SC), finite element models using ANSYS (with large number of elements) and Odegard's proposed analytical model, all presented in [Odegard 2004].

It can be seen that, using only one MTCG, the proposed model gives very accurate predictions as compared to those of Mori–Tanaka's model. It is known that the self-consistent model deviates from Mori–Tanaka's model and gives unrealistic predictions as the volume fraction increases. The proposed method is much more computationally efficient as well as numerically more accurate than the simple finite element models (FEM) using ANSYS, and can be used to model piezo-composites even if the arrangement of particles is not symmetrical which is the main assumption used in all the previously mentioned analytical models.

7.5. Damage detection in porous piezoelectric materials with arbitrary oriented elliptical voids. We consider a porous piezoelectric RVE made of 20 PZT-4 piezoelectric grains with arbitrary sized elliptical

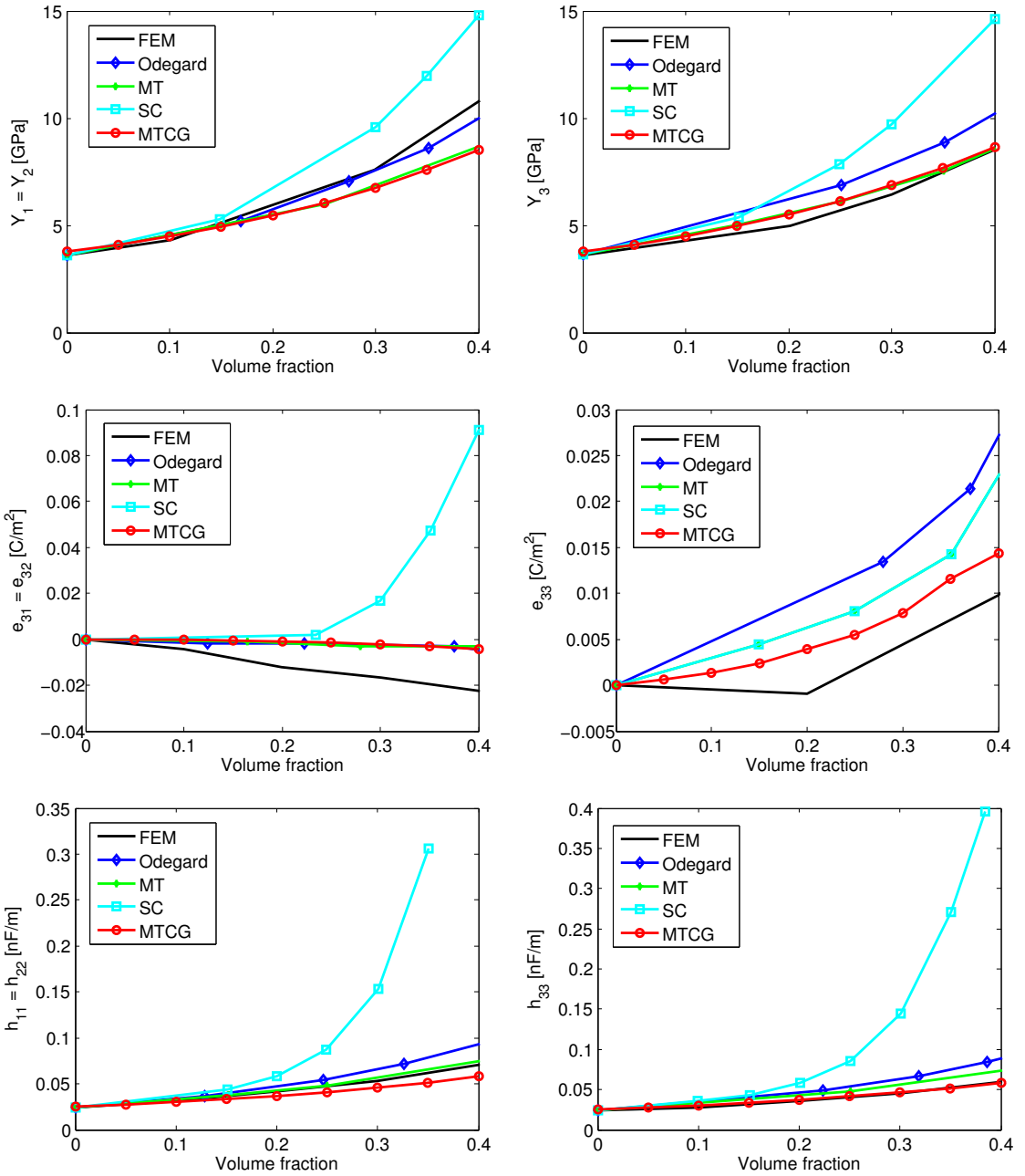


Figure 6. Predictions of effective piezoelectric material properties of PZT-7A/LaRC-SI as functions of particle volume fraction.

voids whose b/a ratios are in the range of 0.7–1.3. The dimensions of the RVE are $L = W = 1$ mm and the porosity volume fraction is 0.05. The direction of polarization is vertically upward in all grains. The lower edge is prevented from motion in the vertical direction while the lower left corner node is electrically grounded and constrained in the horizontal direction. A mechanical loading $\sigma_o = 1$ GPa is

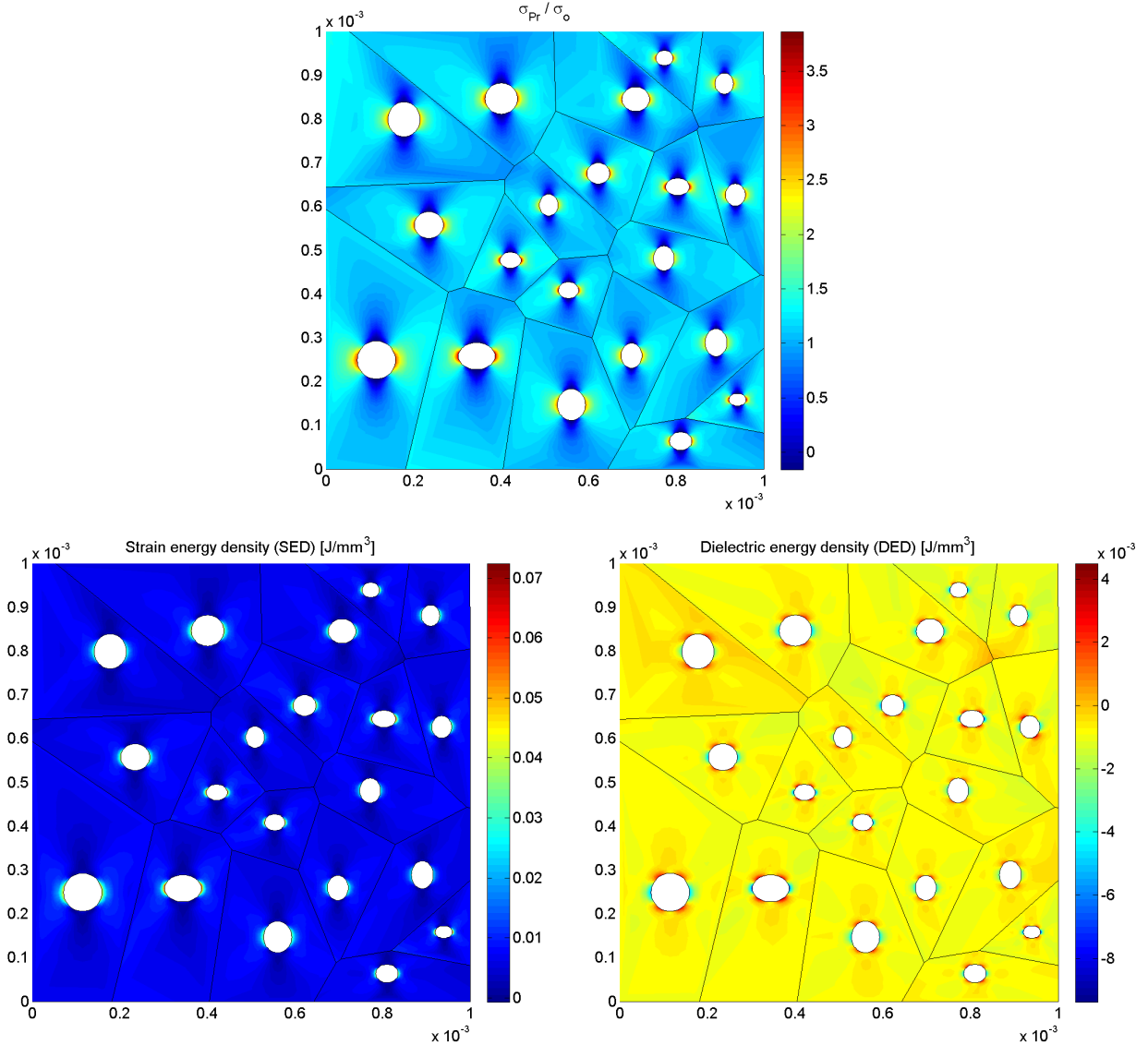


Figure 7. Porous piezoelectric material under mechanical loading: contour plot for principal stress (upper), strain energy density (lower left), and dielectric energy density (lower right).

applied on the upper edge. Contour plots of maximum principal stress, strain energy density (SED), as well as dielectric energy density are shown in [Figure 7](#).

As can be seen from the figures, high principal stress and strain energy density concentrations are observed near the cavities, in the direction perpendicular to the loading direction. On the other hand, at the locations near the voids, in the direction parallel to the loading direction, low stress and strain energy density values are observed. Higher stress and strain energy density concentrations can be observed around voids that have lower values of b/a (because these voids are sharper and are approaching the

shapes of cracks). This gives us an idea about where damage is more likely to initiate and develop in porous piezoelectric materials. It is also interesting to note that the dielectric energy concentrates around the voids at angles $\pm 45^\circ$ from the mechanical loading direction, and decreases around the voids in the direction perpendicular to the loading direction.

In this example there are 44 inner grain boundaries and 17 outer grain boundaries. Since the special solution set is used, the number of collocation equations, according to (40), is $6 \times 44 \times 2 + 3 \times 17 \times 2 = 630$, while the number of unknowns, according to (39), is $20 \times 18 = 360$. Solving the same problem using a finite element analysis software like COMSOL Multiphysics and using regular triangular elements of “normal” size to mesh the problem domain generates 10,163 elements corresponding to 5,360 nodes and 16,080 degrees of freedom. COMSOL has nine levels of element sizes named: extremely coarse, extra coarse, coarser, coarse, normal, fine, finer, extra fine and extremely fine. Refining the mesh by selecting smaller element sizes in order to refine the results will definitely increase the number of nodes and the size of the FE system of equations to be solved. If voids are replaced by inclusions, according to Equations (39) and (40), the number of unknowns will be 1,680 and the number of equations will be 2,550. Solving it using COMSOL requires 12,189 regular elements of “normal” size corresponding to 6,153 nodes and 18,459 degrees of freedom. This is the case for a domain with only 20 voids/inclusions. If it is required to analyze a domain with 200, 2000 or more grains with voids/inclusions in a direct numerical simulation (DNS), the regular finite element method would be highly expensive and impractical as compared to the MTCGs method and the newly developed methods presented in [Bishay and Atluri 2014; Bishay et al. 2014; Dong and Atluri 2012b; 2012c; 2012d].

8. Summary and conclusions

The Lekhnitskii formalism is presented here for the general plane electromechanical problems that can be applied to coupled (piezoelectric) or uncoupled (elastic) materials. Multi-region Trefftz computational grains (MTCGs) method is proposed based on this formalism to model different porous and composite piezoelectric materials in the micro and meso scales where each computational grain has an irregular polygonal shape that resembles the shape of a material grain with arbitrary number of sides and neighboring grains. Each grain also may contain a circular or an arbitrary oriented elliptical void or inclusion, and may have its own direction of polarization. Collocation method is used to enforce the electromechanical natural and essential boundary conditions, continuity and reciprocity conditions along grain boundaries, and void/inclusion interface conditions. Applications of the proposed method include: (1) solving inverse problems by predicting the electromechanical stress at some unreachable locations in structures (like voids) using all the available or measured data even with noise (regularization methods should be used); (2) determining the effective material properties of different piezoelectric composites; (3) optimizing the material properties of piezoelectric composites by controlling the microstructure parameters (shapes of voids/inclusions, orientations, spatial distributions, material properties, etc.); and (4) obtaining the distribution of all secondary fields and the strain and dielectric energy densities in the microstructure to predict locations of damage.

Acknowledgements

This work was funded by the Deanship of Scientific Research (DSR), King Abdulaziz University, under grant number (3-130-35-HiCi). The authors, therefore, acknowledge the technical and financial support of KAU. This research is also supported in part by the Mechanics Section, Vehicle Technology Division, of the US Army Research Labs, under a collaborative research agreement with UCI. The encouragement of Dy Le and Jaret Riddick is thankfully acknowledged.

References

- [Araki and Halloran 2005] K. Araki and J. W. Halloran, “Porous ceramic with interconnected pore channels by a novel freeze casting technique”, *J. Am. Ceram. Soc.* **88**:5 (2005), 1108–1114.
- [Berger et al. 2005] H. Berger, S. Kari, U. Gabbert, R. Rodriguez-Ramos, R. Guinovart-Díaz, J. A. Otero, and J. Bravo-Castillero, “An analytical and numerical approach for calculating effective material coefficients of piezoelectric fiber composites”, *Int. J. Solids Struct.* **42** (2005), 5692–5714.
- [Berger et al. 2006] H. Berger, S. Kari, U. Gabbert, R. Rodriguez-Ramos, J. Bravo-Castillero, R. Guinovart-Díaz, F. J. Sabina, and G. A. Maugin, “Unit cell models of piezoelectric fiber composites for numerical and analytical calculation of effective properties”, *Smart Mater. Struct.* **15** (2006), 451–458.
- [Bishay and Atluri 2012] P. L. Bishay and S. N. Atluri, “High-performance 3D hybrid/mixed, and simple 3D Voronoi cell finite elements, for macro- & micro-mechanical modeling of solids, without using multi-field variational principles”, *Comput. Model. Eng. Sci.* **84**:1 (2012), 41–97.
- [Bishay and Atluri 2013] P. L. Bishay and S. N. Atluri, “2D and 3D multiphysics Voronoi cells, based on radial basis functions, for direct mesoscale numerical simulation (DMNS) of the switching phenomena in ferroelectric polycrystalline materials”, *Comput. Mater. Continua* **33**:1 (2013), 19–62.
- [Bishay and Atluri 2014] P. L. Bishay and S. N. Atluri, “Treffitz–Lekhnitski grains (TLGs) for efficient direct numerical simulation (DNS) of the micro/meso mechanics of porous piezoelectric materials”, *Comput. Mater. Sci.* **83** (2014), 235–249.
- [Bishay et al. 2014] P. L. Bishay, L. Dong, and S. N. Atluri, “Multi-physics computational grains (MPCGs) for direct numerical simulation (DNS) of piezoelectric composite/porous materials and structures”, *Comput. Mech.* (2014). Accepted for publication.
- [Cao et al. 2013] C. Cao, A. Yu, and Q.-H. Qin, “A new hybrid finite element approach for plane piezoelectricity with defects”, *Acta Mech.* **224**:1 (2013), 41–61.
- [Chung and Ting 1996] M. Y. Chung and T. C. T. Ting, “Piezoelectric solid with an elliptic inclusion or hole”, *Int. J. Solids Struct.* **33**:23 (1996), 3343–3361.
- [Dong and Atluri 2012a] L. Dong and S. N. Atluri, “A simple multi-source-point Treffitz method for solving direct/inverse SHM problems of plane elasticity in arbitrary multiply-connected domains”, *Comput. Model. Eng. Sci.* **85**:1 (2012), 1–43.
- [Dong and Atluri 2012b] L. Dong and S. N. Atluri, “T-Treffitz Voronoi cell finite elements with elastic/rigid inclusions or voids for micromechanical analysis of composite and porous materials”, *Comput. Model. Eng. Sci.* **83**:2 (2012), 183–220.
- [Dong and Atluri 2012c] L. Dong and S. N. Atluri, “Development of 3D T-Treffitz Voronoi cell finite elements with/without spherical voids &/or elastic/rigid inclusions for micromechanical modeling of heterogeneous materials”, *Comput. Mater. Continua* **29**:2 (2012), 169–211.
- [Dong and Atluri 2012d] L. Dong and S. N. Atluri, “Development of 3D Treffitz Voronoi cells with ellipsoidal voids &/or elastic/rigid inclusions for micromechanical modeling of heterogeneous materials”, *Comput. Mater. Continua* **30**:1 (2012), 39–82.
- [Dong and Atluri 2012e] L. Dong and S. N. Atluri, “SGBEM (using non-hyper-singular traction BIE), and super elements, for non-collinear fatigue-growth analyses of cracks in stiffened panels with composite-patch repairs”, *Comput. Model. Eng. Sci.* **89**:5 (2012), 417–458.

- [Dong and Atluri 2013] L. Dong and S. N. Atluri, “SGBEM Voronoi cells (SVCs), with embedded arbitrary-shaped inclusions, voids, and/or cracks, for micromechanical modeling of heterogeneous materials”, *Comput. Mater. Continua* **33**:2 (2013), 111–154.
- [Hansen 1994] P. C. Hansen, “Regularization tools: a Matlab package for analysis and solution of discrete ill-posed problems”, *Numer. Algorithms* **6**:1-2 (1994), 1–35.
- [Jin et al. 2003] D. R. Jin, Z. Y. Meng, and F. Zhou, “Mechanism of resistivity gradient in monolithic PZT ceramics”, *Mater. Sci. Eng. B* **99** (2003), 83–87.
- [Kari et al. 2008] S. Kari, H. Berger, and U. Gabbert, “Numerical evaluation of effective material properties of piezoelectric fibre composites”, pp. 109–120 in *Micro-macro-interactions: in structured media and particle systems*, edited by A. Bertram and J. Tomas, Springer, Berlin, 2008.
- [Klicker et al. 1981] K. A. Klicker, J. V. Biggers, and R. E. Newnham, “Composites of PZT and epoxy for hydrostatic transducer applications”, *J. Am. Ceram. Soc.* **64** (1981), 5–9.
- [Kumar et al. 2006] B. P. Kumar, H. H. Kumar, and D. K. Kharat, “Effect of porosity on dielectric properties and microstructure of porous PZT ceramics”, *Mater. Sci. Eng. B* **127** (2006), 130–133.
- [Lekhnitskii 1957] S. G. Lekhnitskii, *Анизотропные пластинки*, 2nd ed., Gostekhidat, Moscow, 1957. Translated as *Anisotropic plates*, Gordon and Breach, New York, 1968.
- [Lekhnitskii 1977] S. G. Lekhnitskii, *Теория упругости анизотропного тела*, 2nd ed., Nauka, Moscow, 1977. Translated as *Theory of elasticity of an anisotropic body*, Mir, Moscow, 1981.
- [Li et al. 2001] J. F. Li, K. Takagi, N. Terakubo, and R. Watanabe, “Electrical and mechanical properties of piezoelectric ceramic/metal composites in the Pb(Zr, Ti)O₃/Pt system”, *Appl. Phys. Lett.* **79** (2001), 2441–2443.
- [Li et al. 2003] J. F. Li, K. Takagi, M. Ono, W. Pan, R. Watanabe, and A. Almajid, “Fabrication and evaluation of porous piezoelectric ceramics and porosity-graded piezoelectric actuators”, *J. Am. Ceram. Soc.* **86** (2003), 1094–1098.
- [Lu and Williams 1998] P. Lu and F. W. Williams, “Green functions of piezoelectric material with an elliptic hole or inclusion”, *Int. J. Solids Struct.* **35** (1998), 651–664.
- [Moorthy and Ghosh 1996] S. Moorthy and S. Ghosh, “A model for analysis of arbitrary composite and porous microstructures with Voronoi cell finite elements”, *Int. J. Numer. Methods Eng.* **39** (1996), 2363–2398.
- [Odegard 2004] G. M. Odegard, “Constitutive modeling of piezoelectric polymer composites”, *Acta Mater.* **52**:18 (2004), 5315–5330.
- [Piltner 1985] R. Piltner, “Special finite elements with holes and internal cracks”, *Int. J. Numer. Methods Eng.* **21**:8 (1985), 1471–1485.
- [Piltner 2008] R. Piltner, “Some remarks on finite elements with an elliptic hole”, *Finite Elem. Anal. Des.* **44**:12-13 (2008), 767–772.
- [Sheng et al. 2006] N. Sheng, K. Y. Sze, and Y. K. Cheung, “Trefftz solutions for piezoelectricity by Lekhnitskii’s formalism and boundary collocation method”, *Int. J. Numer. Methods Eng.* **65** (2006), 2113–2138.
- [Sosa 1991] H. Sosa, “Plane problems in piezoelectric media with defects”, *Int. J. Solids Struct.* **28**:4 (1991), 491–505.
- [Stroh 1958] A. N. Stroh, “Dislocations and cracks in anisotropic elasticity”, *Philos. Mag.* (8) **3**:30 (1958), 625–646.
- [Tikhonov and Arsenin 1974] A. N. Tikhonov and V. Y. Arsenin, *Методы решения некорректных задач*, Nauka, Moscow, 1974. Translated as *Solutions of ill-posed problems*, Winston, Washington, DC, 1977.
- [Wang and Qin 2012] H. Wang and Q.-H. Qin, “A new special element for stress concentration analysis of a plate with elliptical holes”, *Acta Mech.* **223**:6 (2012), 1323–1340.
- [Wang et al. 2004] X. W. Wang, Y. Zhou, and W. L. Zhou, “A novel hybrid finite element with a hole for analysis of plane piezoelectric medium with defects”, *Int. J. Solids Struct.* **41** (2004), 7111–7128.
- [Xu and Rajapakse 1998] X. L. Xu and R. K. N. D. Rajapakse, “Boundary element analysis of piezoelectric solids with defects”, *Compos. B Eng.* **29**:5 (1998), 655–669.
- [Xu and Rajapakse 1999] X. L. Xu and R. K. N. D. Rajapakse, “Analytical solution for an arbitrarily oriented void/crack and fracture of piezoceramics”, *Acta Mater.* **47** (1999), 1735–1747.

[Zhang and Katsube 1995] J. Zhang and N. Katsube, “A hybrid finite element method for heterogeneous materials with randomly dispersed rigid inclusions”, *Int. J. Numer. Methods Eng.* **38** (1995), 1635–1653.

[Zhang and Katsube 1997] J. Zhang and N. Katsube, “A polygonal element approach to random heterogeneous media with rigid ellipses or elliptic voids”, *Comput. Methods Appl. Mech. Eng.* **148** (1997), 225–234.

Received 7 Dec 2013. Revised 10 Apr 2014. Accepted 8 May 2014.

PETER L. BISHAY: PBishay@stmartin.edu

Center for Aerospace Research and Education (CARE), The Henry Samueli School of Engineering, University of California, Irvine, 4200 Engineering Gateway, Irvine, CA 92697, United States

and

The Hal and Inge Marcus School of Engineering, Saint Martin’s University, 5000 Abbey Way SE, OM 329, Lacey, WA 98503-7500, United States

ABDULLAH ALOTAIBI: aalotaibi@kau.edu.sa

Department of Mathematics, Faculty of Sciences, King Abdulaziz University, P.O. Box 80203, Jeddah 21589, Saudi Arabia

SATYA N. ATLURI: satluri@uci.edu

Center for Aerospace Research and Education (CARE), The Henry Samueli School of Engineering, University of California, Irvine, 4200 Engineering Gateway, Irvine, CA 92697, United States

and

Faculty of Engineering, King Abdulaziz University, Jeddah 22254, Saudi Arabia

JOURNAL OF MECHANICS OF MATERIALS AND STRUCTURES

msp.org/jomms

Founded by Charles R. Steele and Marie-Louise Steele

EDITORIAL BOARD

ADAIR R. AGUIAR	University of São Paulo at São Carlos, Brazil
KATIA BERTOLDI	Harvard University, USA
DAVIDE BIGONI	University of Trento, Italy
IWONA JASIUK	University of Illinois at Urbana-Champaign, USA
THOMAS J. PENCE	Michigan State University, USA
YASUhide SHINDO	Tohoku University, Japan
DAVID STEIGMANN	University of California at Berkeley

ADVISORY BOARD

J. P. CARTER	University of Sydney, Australia
D. H. HODGES	Georgia Institute of Technology, USA
J. HUTCHINSON	Harvard University, USA
D. PAMPLONA	Universidade Católica do Rio de Janeiro, Brazil
M. B. RUBIN	Technion, Haifa, Israel

PRODUCTION production@msp.org

SILVIO LEVY Scientific Editor

See msp.org/jomms for submission guidelines.

JoMMS (ISSN 1559-3959) at Mathematical Sciences Publishers, 798 Evans Hall #6840, c/o University of California, Berkeley, CA 94720-3840, is published in 10 issues a year. The subscription price for 2014 is US \$555/year for the electronic version, and \$710/year (+\$60, if shipping outside the US) for print and electronic. Subscriptions, requests for back issues, and changes of address should be sent to MSP.

JoMMS peer-review and production is managed by EditFLOW[®] from Mathematical Sciences Publishers.

PUBLISHED BY

 **mathematical sciences publishers**
nonprofit scientific publishing
<http://msp.org/>

© 2014 Mathematical Sciences Publishers

B-splines collocation eigenanalysis of 2D acoustic problems CHRISTOPHER G. PROVATIDIS	259
Multi-region Trefftz collocation grains (MTCGs) for modeling piezoelectric composite and porous materials in direct and inverse problems PETER L. BISHAY, ABDULLAH ALOTAIBI and SATYA N. ATLURI	287
Analytical solution for ductile and FRC plates on elastic ground loaded on a small circular area ENRICO RADI and PIETRO DI MAIDA	313
Solution of a receding contact problem using an analytical method and a finite element method ERDAL ÖNER, MURAT YAYLACI and AHMET BIRINCI	333
Sliding of a cup-shaped die on a half-space: influence of thermal relaxation, convection and die temperature LOUIS MILTON BROCK	347